Measurements and interpretations of STXS and differential and fiducial cross sections in HWW* channel with the ATLAS detector

Dongshuo Du (杜东硕)

University of Science and Technology of China

(On behalf of the ATLAS collaboration)

Higgs 2023, Nov 27- Dec 2 2023, Beijing

Outline

- Introduction
- Inclusive cross sections of Higgs boson production
  - ggF+VBF with $H \to WW^*$ Phys. Rev. D 108 (2023) 032005
  - VH with $H \to WW^*$ ATLAS-CONF-2022-067
- Fiducial and differential cross sections
  - ggF with $H \to WW^* \to e\nu\mu\nu$ Eur. Phys. J. C 83 (2023) 774
  - VBF with $H \to WW^* \to e\nu\mu\nu$ Phys. Rev. D 108 (2023) 072003
- Summary

Outline

- Introduction

- Inclusive cross sections of Higgs boson production
  - ggF+VBF with $H \to WW^*$ Phys. Rev. D 108 (2023) 032005
  - VH with $H \to WW^*$ ATLAS-CONF-2022-067

- Fiducial and differential cross sections
  - ggF with $H \to WW^* \to e\nu\mu\nu$ Eur. Phys. J. C 83 (2023) 774
  - VBF with $H \to WW^* \to e\nu\mu\nu$ Phys. Rev. D 108, 072003

- Summary

Introduction

➢ A particle consistent with the SM Higgs boson was discovered at the LHC in 2012 with a mass of ~125 GeV

arXiv: 2209.07510

➢ The Higgs boson is one of the most important particles in the SM

- Connected to the numerous fundamental questions
- A detailed study of its properties may provide answers

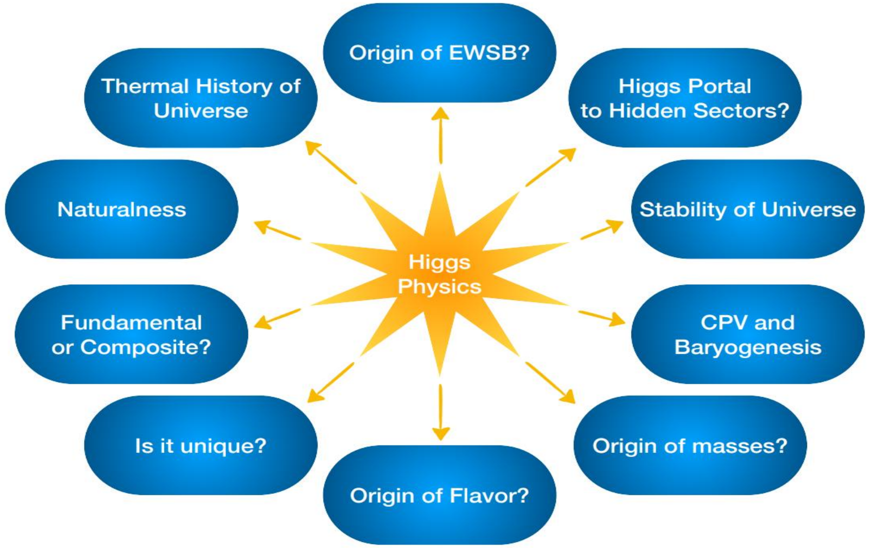

➢ The measurement of production and decay rates is one of the most important way to test the SM and look for possible new physics.

- Inclusive cross section of Higgs production & decay
- Simplified template cross-sections (STXS) measurement
- Fiducial and differential cross section measurement

With increasing data, measurements can be performed with finer binning and in a more model-independent way

Higgs production and decay modes

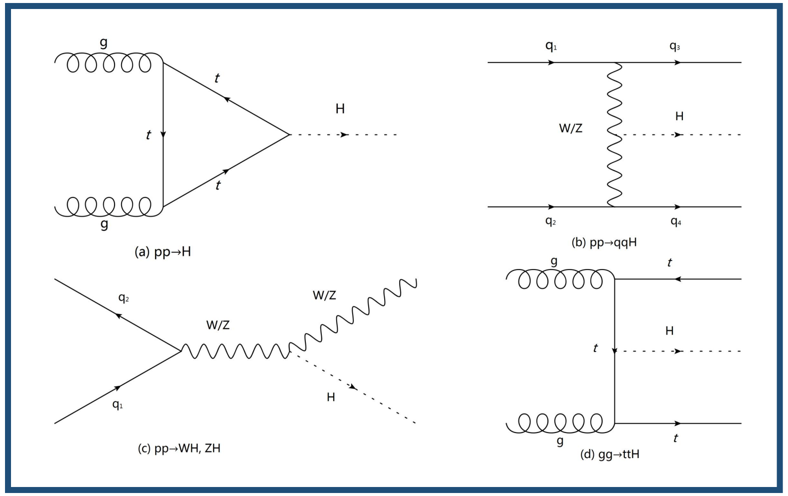

Production modes

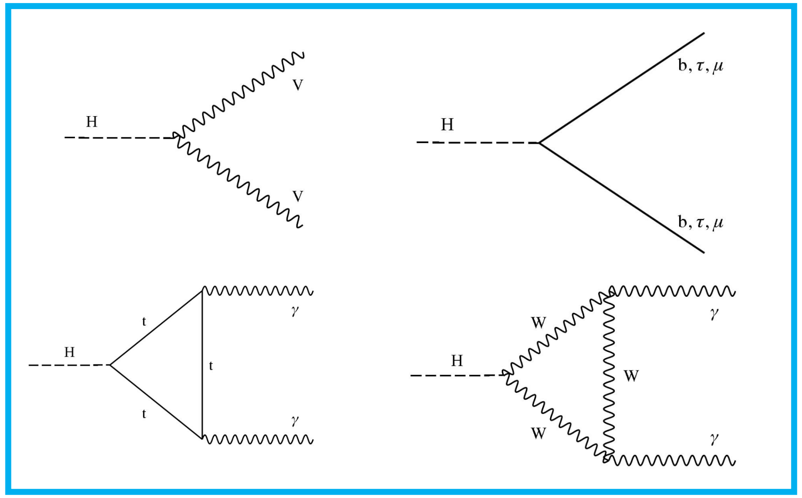

Decay modes

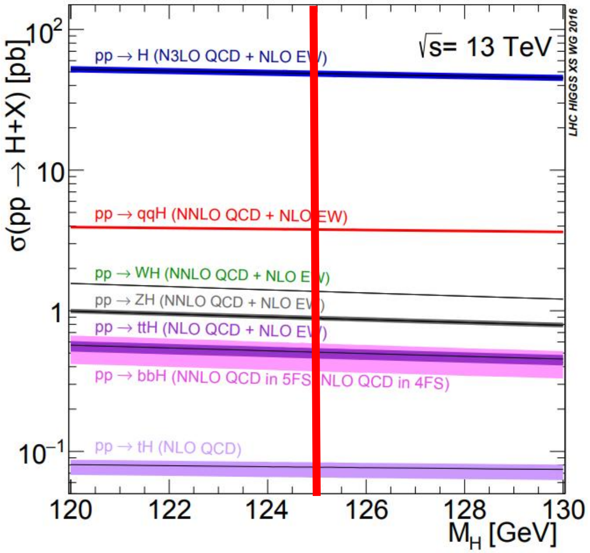

ggF: 87%

VBF: 7%

VH: 4%

ttH: 2%

- ➢ The leading production mode is ggF
- ➢ Followed by VBF and VH production modes
- ➢ ttH can provide direct measurement of top-Higgs coupling
- ➢ H →bb (57%) : The most profilic channel, very hard to observe
- ➢ H→WW* (21%): The second largest BR, large background but leptonic decay useful for distinguishing signal
- ➢ H→γγ (0.2%) and H→ZZ*→4l (0.01%): Small BR but cleaner background

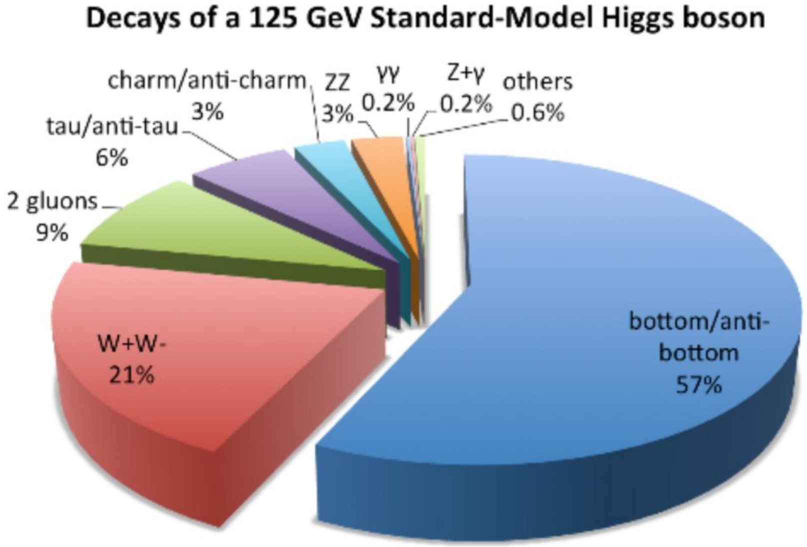

Higgs production and decay modes

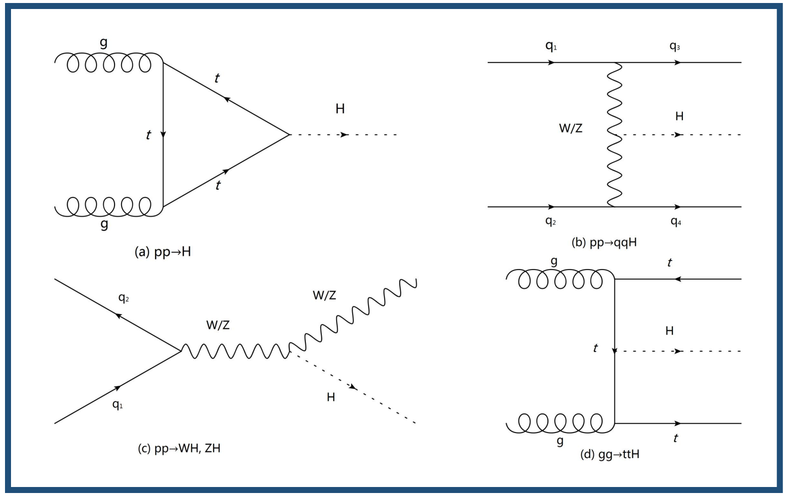

Production modes

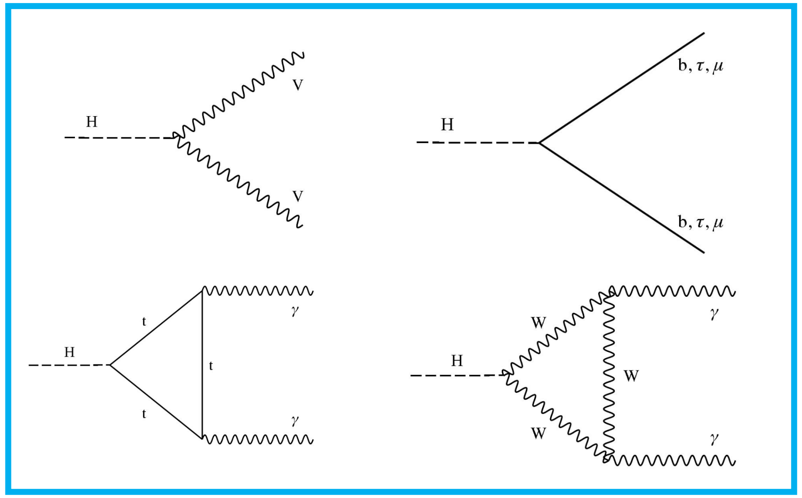

Decay modes

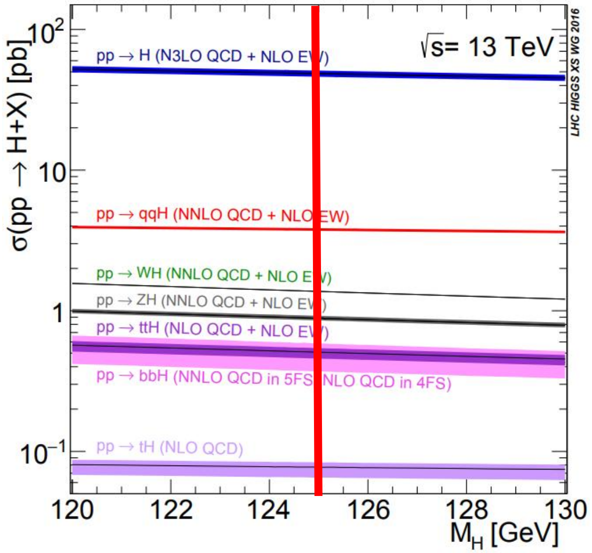

ggF: 87%

VBF: 7%

VH: 4%

ttH: 2%

- The leading production mode is ggF ★
- Followed by VBF and VH production modes ★
- ttH can provide direct measurement of top-Higgs coupling
- H →bb (58%) : The most profilic channel, very hard to observe
- H→WW* (21%): The second largest BR, large background but leptonic decay useful for distinguishing signal ★
- H→γγ (0.2%) and H→ZZ*→4l (0.01%): Small BR but cleaner background

Topic today

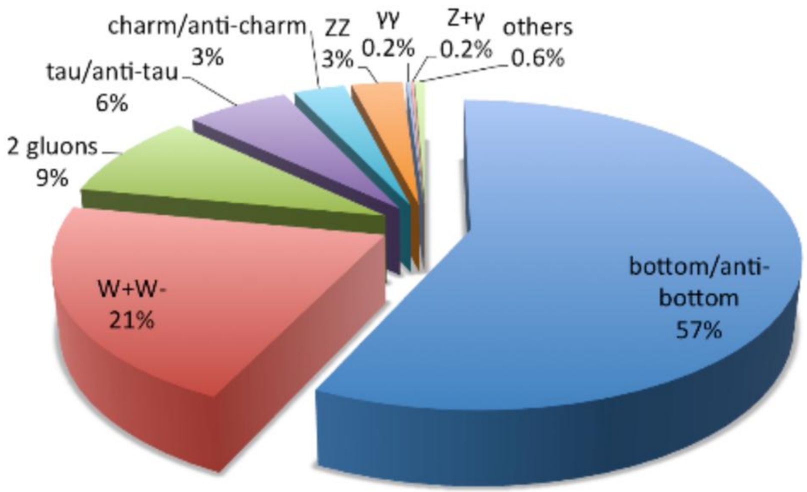

Outline

- Introduction

- Inclusive cross sections of Higgs boson production
  - ggF+VBF with $H \rightarrow WW^*$ Phys. Rev. D 108 (2023) 032005
  - VH with $H \rightarrow WW^*$ ATLAS-CONF-2022-067

- Fiducial and differential cross sections
  - ggF with $H \rightarrow WW^* \rightarrow e\nu\mu\nu$ Eur. Phys. J. C 83 (2023) 774
  - VBF with $H \rightarrow WW^* \rightarrow e\nu\mu\nu$ Phys. Rev. D 108, 072003

- Summary

ggF + VBF H→WW*: Analysis Strategy

- Signal: different flavour (eμ+μe) opposite charge leptons + MET

Phys. Rev. D 108 (2023) 032005

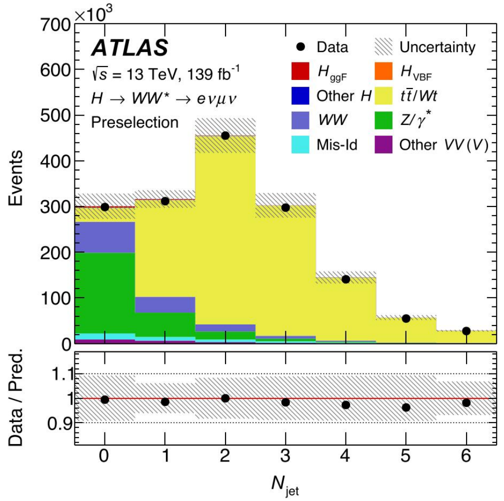

- Events split in 4 analysis categories based on N_{jets}
  - ggF: $N_{jets} = 0, 1, \geq 2$, cut based
    - ✓ m_T used as discriminant variable
  - VBF: $N_{jets} \geq 2$, "deep" neural network (DNN) based
    - ✓ DNN used as discriminant variable

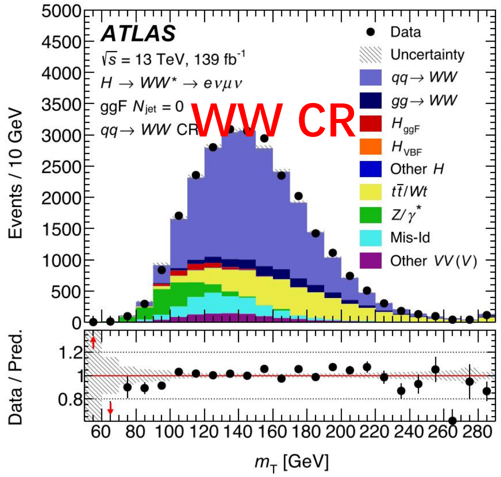

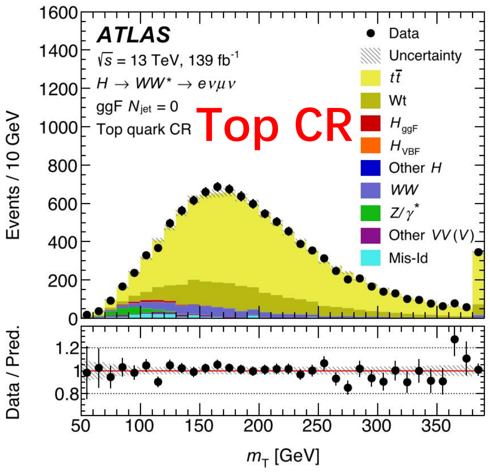

- Main background:
  - Non-resonant qqWW, top and Z→ττ
    - ✓ ggF: qqWW, top and Z→ττ normalized by CRs
    - ✓ VBF: top and Z→ττ normalized by CRs
  - Background with mis-identified leptons estimated by data-driven fake factor method

$$m_T = \sqrt{(E_T^{\ell\ell} + E_T^{\text{miss}})^2 - |\boldsymbol{p}_T^{\ell\ell} + \boldsymbol{E}_T^{\text{miss}}|^2}, \quad E_T^{\ell\ell} = \sqrt{|\boldsymbol{p}_T^{\ell\ell}|^2 + m_{\ell\ell}^2}$$

ggF + VBF H→WW*: Coupling results

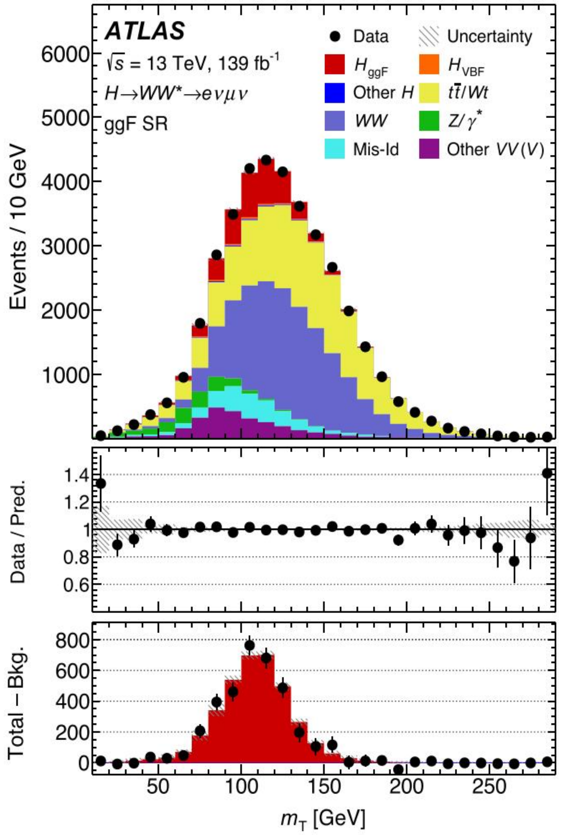

- Post fit M_T distribution in the ggF combined SR

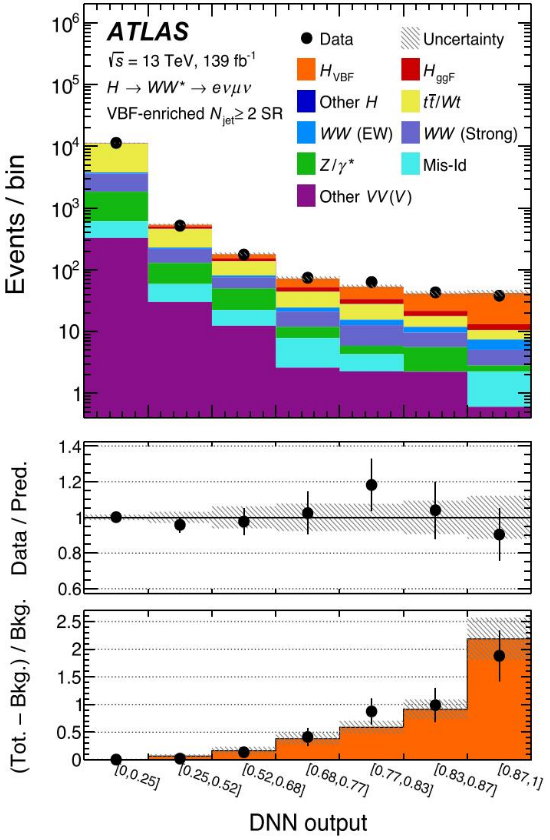

- Post fit BDT distribution in the VBF SR

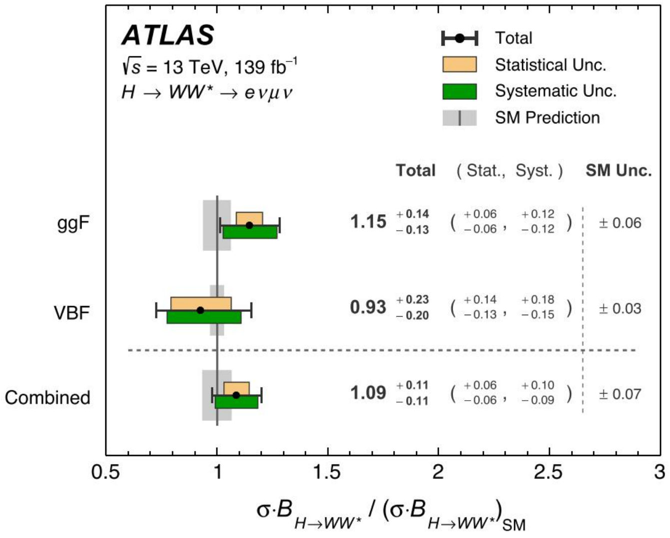

[Phys. Rev. D 108 (2023) 032005]

- ➢ Results from simultaneous fit to all SRs + CRs
- ➢ Dominanted by systematic uncertainties

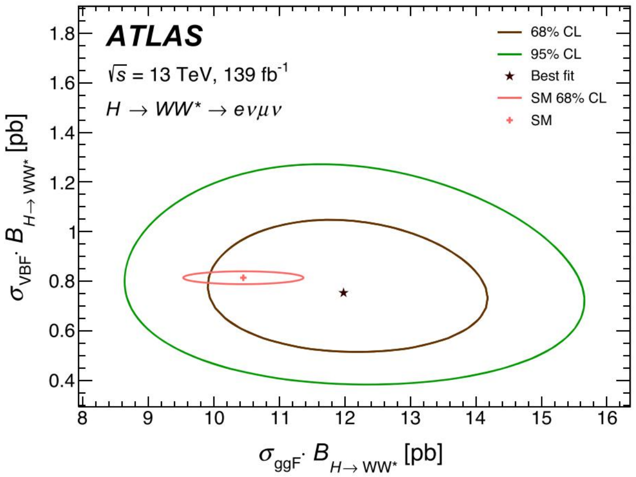

$$\sigma_{\rm ggF}\cdot\mathcal{B}_{H\to WW^*} = 12.0\pm 1.4\ \text{pb}$$
$$= 12.0\pm 0.6(\text{stat})^{+0.9}_{-0.8}(\text{exp syst})^{+0.6}_{-0.5}$$
$$\times(\text{sig theo})\pm 0.8(\text{bkg theo})\ \text{pb}$$

$$\sigma_{\rm VBF}\cdot\mathcal{B}_{H\to WW^*} = 0.75^{+0.19}_{-0.16}\ \text{pb}$$
$$= 0.75\pm 0.11(\text{stat})^{+0.07}_{-0.06}(\text{exp syst})^{+0.12}_{-0.08}$$
$$\times(\text{sig theo})^{+0.07}_{-0.06}(\text{bkg theo})\ \text{pb},$$

Good agreement between data and mc prediction

Measurements are consistent with SM prediction

Simplified Template Cross Section (STXS)

- The aim with STXS method:
  - Improve sensitivity of measurements
  - Reduce their dependence on the theory
  - High p_T^H bins more sensitive to beyond standard model effects

- STXS framework provides different stages (e.g. stage 0, stage 1, stage 1.2) with varying degrees of granularity

- Categorizing events into bins of key (truth) variables (p_T^H, N_{jets}, m_{jj}) in different production modes (ggH, EW qqH, VH and ttH)

- STXS well-suited to combine different decay channels

- Higgs boson properties measured with 139 fb^{-1} for Higgs boson rapidity $|y_H| < 2.5$

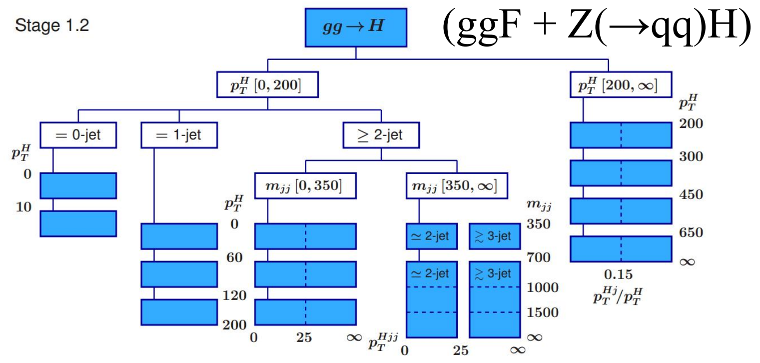

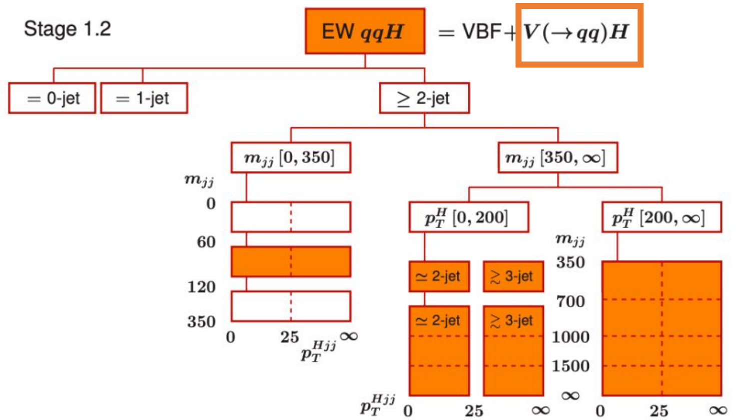

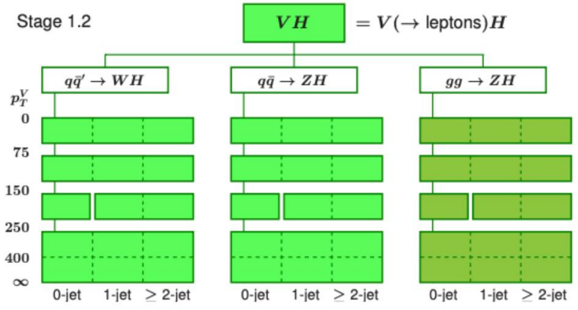

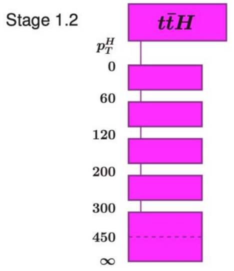

ggF + VBF H→WW*: STXS

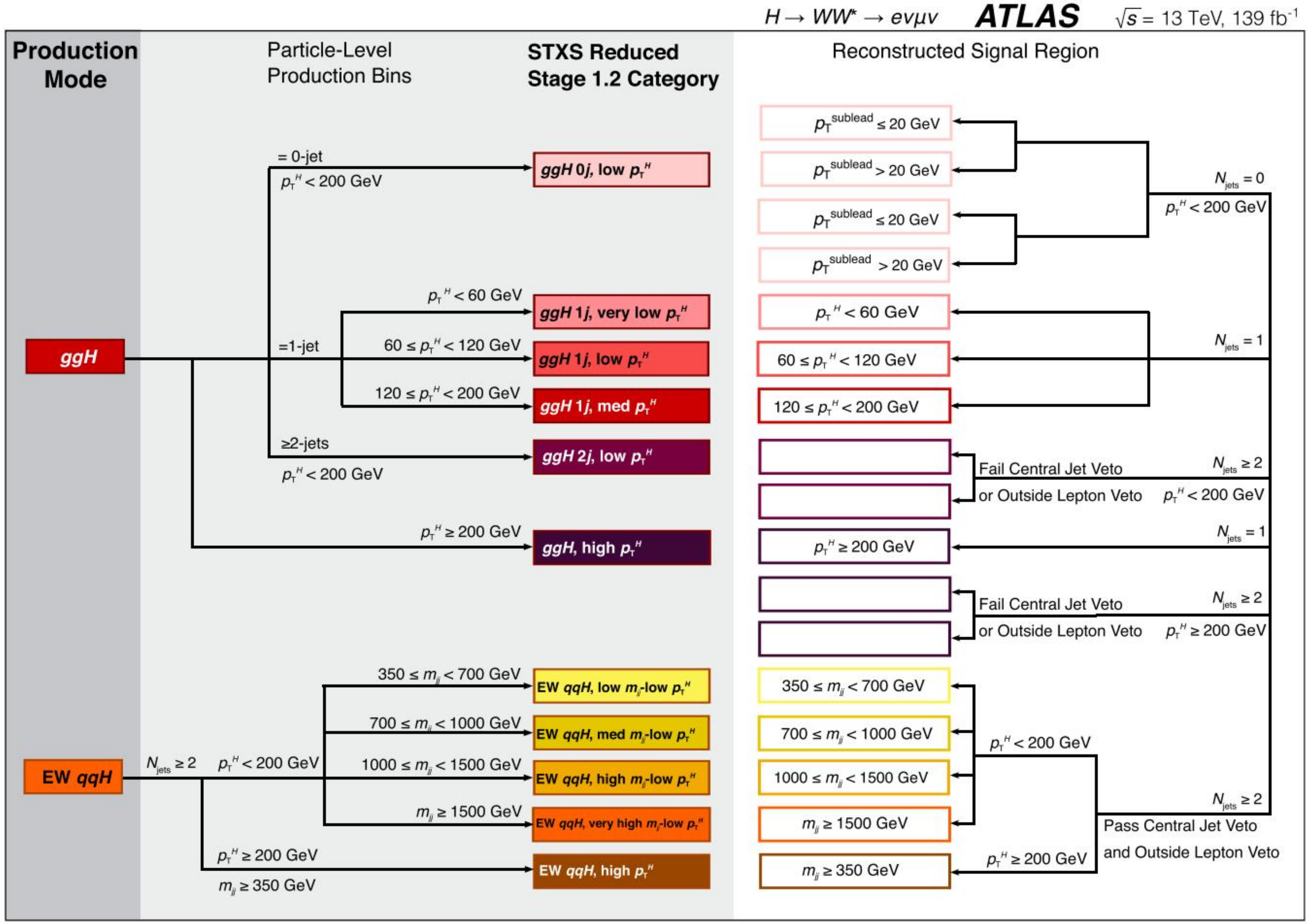

$$p_T^H = |\boldsymbol{p}_T^{\ell\ell} + \boldsymbol{E}_T^{\text{miss}}|$$

Phys. Rev. D 108 (2023) 032005

- This analysis is based on a reduced stage 1.2 categorization scheme to ensure sensitivity for all measurements.
- Split by p_T^H, N_{jets}, m_{jj} into 11 categories
  - 6 bins for ggH and 5 for EW qqH

→ 17 signal regions

- CRs split similar to SRs where statistics allow

→ 27 control regions

ggF + VBF H→WW*: STXS results

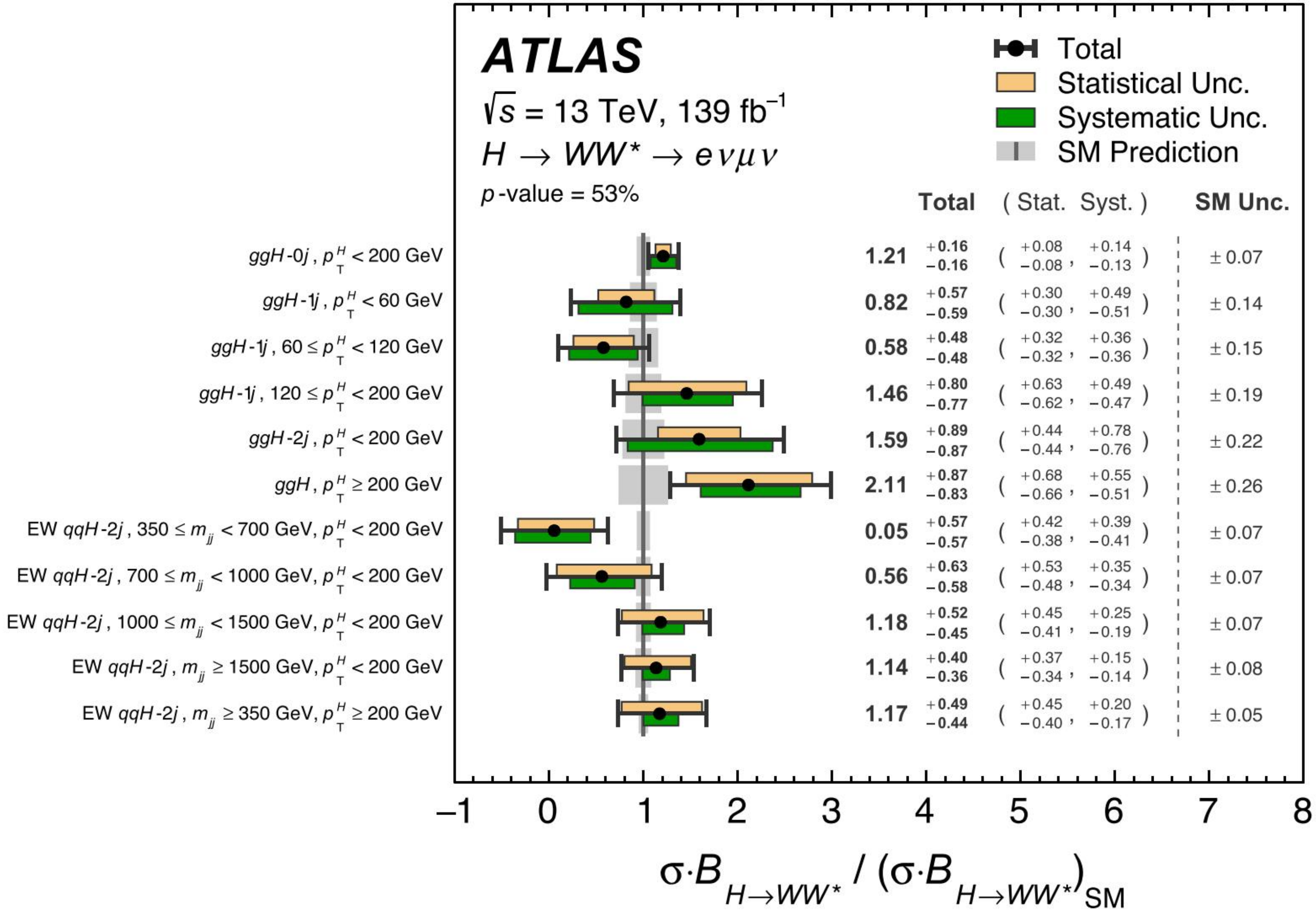

[Phys. Rev. D 108 (2023) 032005]

- Extracted by profile likelihood fit: 17 SRs (m_T/DNN) + 27 CRs
- ggH uncertainties limited by both stat. + syst. uncertainty
- qqH uncertainties limited by statistical uncertainty at high m_{jj} / p_T^H
- Compatible with the SM predictions with a p-value of 53%

VH H→WW* (lvjj, lvlv): Analysis strategy

- Targeting WH and ZH productions: 2, 3 and 4 leptons in the final state
- 8 SRs according to the number, flavour and charges of the leptons
  - **Opposite sign 2l channel** (VH, V→qq) (DNN)
  - **Same sign 2l channel** (WH): ee, mm, em (RNN(*))
  - **3l channel** (WH): Z-depleted/enriched (DNN)
  - **4l channel** (ZH): >= 1 SFOS(**) pair (BDT)
    - ✓ 3m1e + 3e1m: 1 SFOS → highest sensitivity
    - ✓ 4e + 4m + 2e2m: 2SFOS
- Use of MVA techniques to separate Higgs signal from main SM backgrounds for all channels

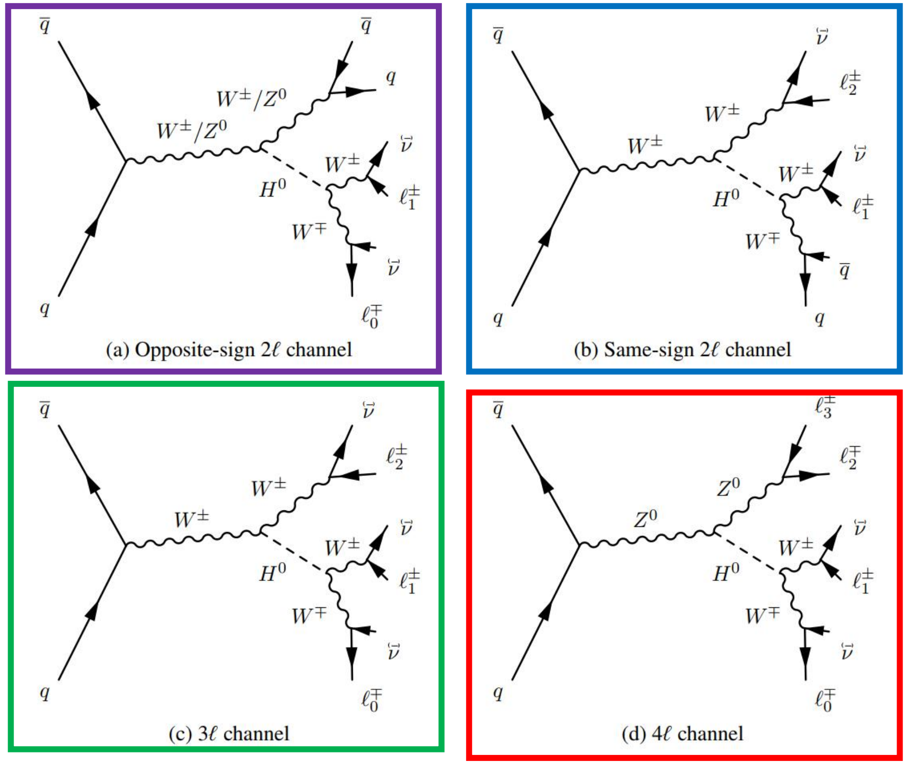

(a) Opposite-sign 2ℓ channel

(b) Same-sign 2ℓ channel

(c) 3ℓ channel

(d) 4ℓ channel

ATLAS-CONF-2022-067

(*) RNN: recurrent neural network

(**) SFOS: same-flavour, opposite-sign

VH H→WW* (lvjj, lvlv): Results

➢Observed VH combined significance: 4.6 σ

- 4l (1 SFOS) is the most sensitive channel
- **Strong evidence** (almost observation) of ZH(→WW*): **4.6σ**

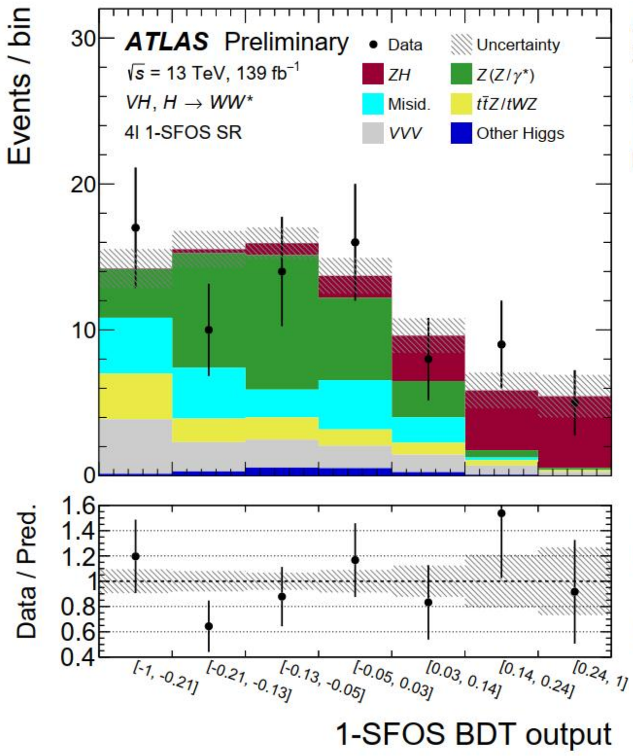

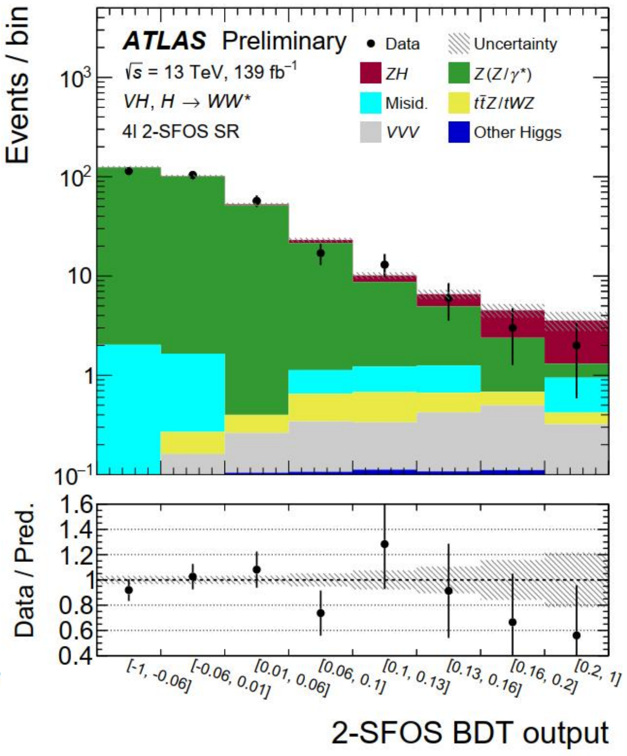

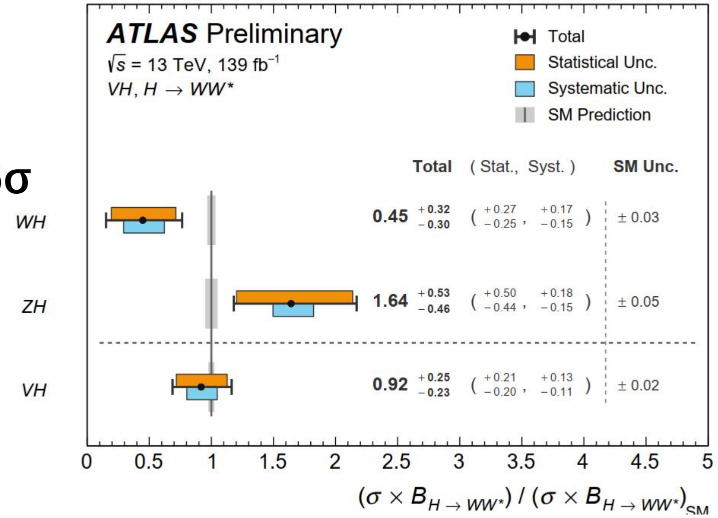

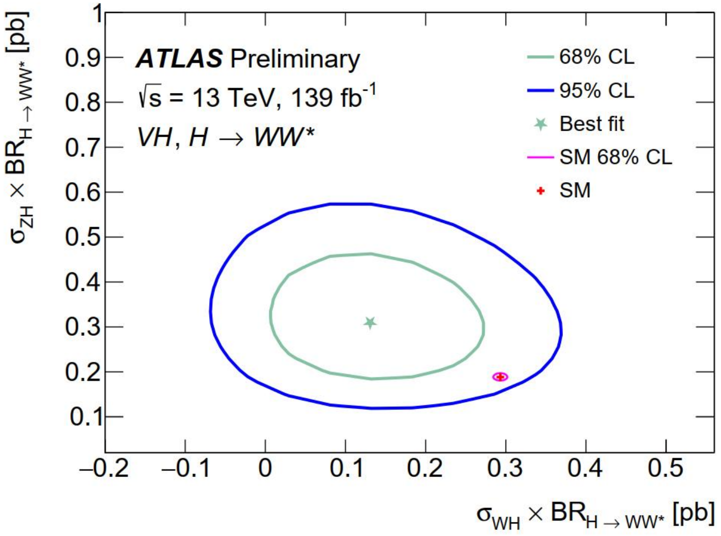

- Dominated by the statistical uncertainty
- The measurements of WH and ZH are compatible at a level of 2.1σ
- Results in agreement with SM within 1.8σ

ATLAS-CONF-2022-067

Most sensitive channels limited by statistics ⟶ **will highly benefit from new Run 3 data**

Outline

- Introduction
- Inclusive cross sections of Higgs boson production
  - ggF+VBF with $H \rightarrow WW^*$ Phys. Rev. D 108 (2023) 032005
  - VH with $H \rightarrow WW^*$ ATLAS-CONF-2022-067
- Fiducial and differential cross sections
  - ggF with $H \rightarrow WW^* \rightarrow e\nu\mu\nu$ Eur. Phys. J. C 83 (2023) 774
  - VBF with $H \rightarrow WW^* \rightarrow e\nu\mu\nu$ Phys. Rev. D 108, 072003
- Summary

Fiducial Differential Cross-section measurement

- With more data collected, the properties of the Higgs boson can be studied in more detail and in a more model independent way

- Fiducial phase space is defined to mimic the real detector acceptance and to minimize the extrapolation effects.

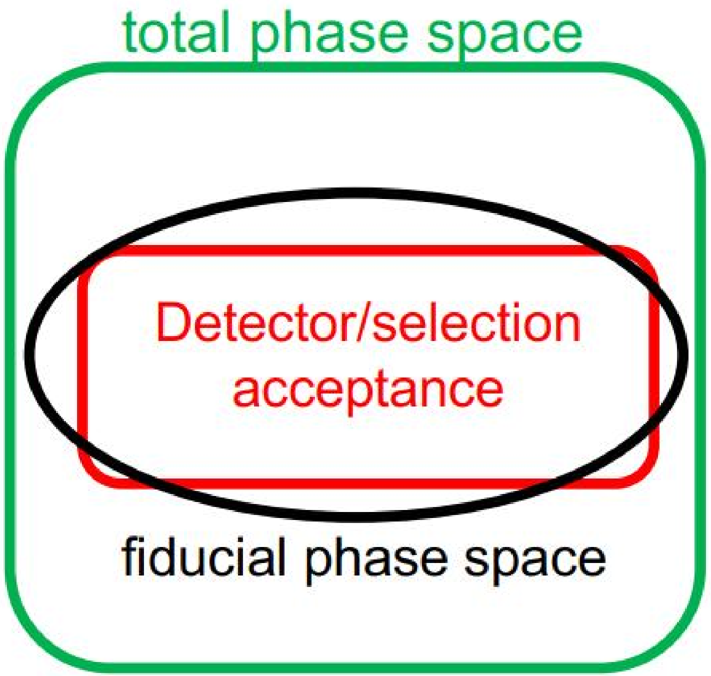

- Limitation:
  - Extrapolation to the total phase space is needed to do the combination
  - Reduced sensitivity for BSM effects compared to dedicated analyses

- Usually considered observables:
  - Higgs boson kinematics & decay observables
  - Jets associated with the Higgs boson

Differential XS in H→WW*: ggF phase space

- Phase space: <= 1 jet

Eur. Phys. J. C 83 (2023) 774

- Various observables in one and two-dimensions are measured to probe different Higgs properties:
  - 8 observables for 1 dimension:
    $|y_{ll}|$, p_T^{ll} , p_T^{l0} , $\Delta\phi_{ll}$, y_{j0} , $cos\theta^*$, p_T^H , m_{ll}
  - 6 observables for 2 dimensions:
    $|y_{ll}|$, p_T^{ll} , p_T^{l0}, $\Delta\phi_{ll}$, $cos\theta^*$, m_{ll} as function of N_{jets}

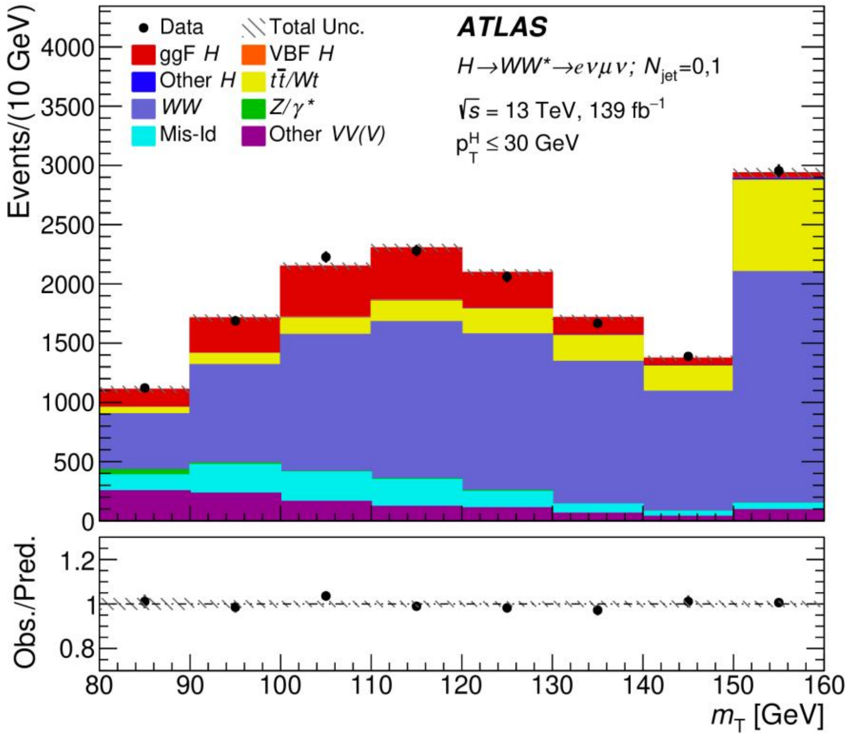

- m_T distribution is used to extract signal in each bin of a given observable, with control regions for background estimation

- Tikhonov-regularized in-likelihood unfolding used

Differential XS in H→WW*: ggF Results

Sensitive to the spin structure

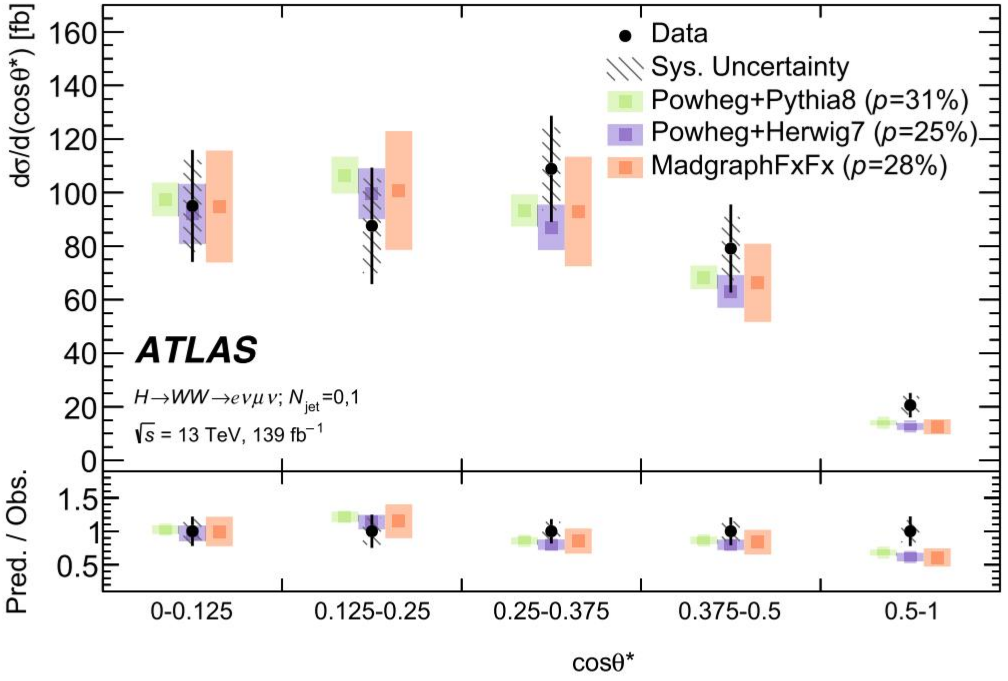

Sensitive to BSM contributions

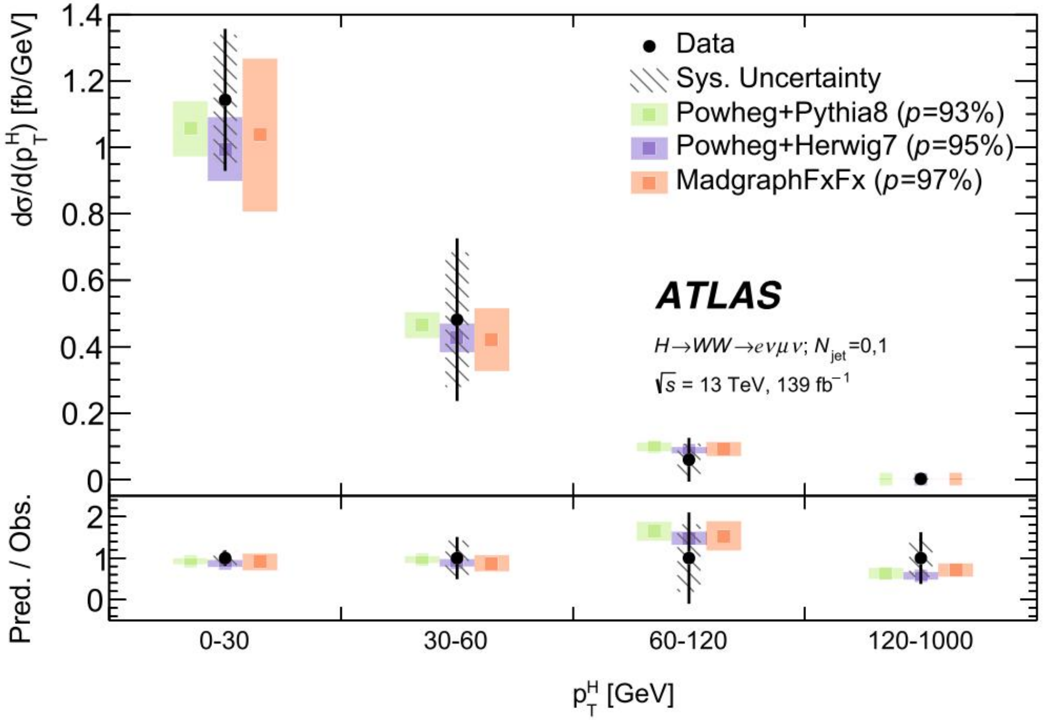

- In general, good agreement between different theoretical predicatons and measured cross sections
- Competitive channel at high Higgs p_T: ~1σ sensitivity for p_T^H > 120 GeV

Differential XS in H→WW*: VBF phase space

- Phase space: >= 2 jet

Phys. Rev. D 108 (2023) 072003

- Differential cross-sections measured for different observables:
  - Higgs related: p_T^H $p_T^{\ell\ell}$ $p_T^{\ell_1}$ $p_T^{\ell_2}$ $m_{\ell\ell}$ $|\Delta y_{\ell\ell}|$ $|\Delta\phi_{\ell\ell}|$ $\cos(\theta_\eta^*)$
  - Jet related: $p_T^{j_1}$ $p_T^{j_2}$ m_{jj} $|\Delta y_{jj}|$ $\Delta\phi_{jj}$

- Dedicated BDT discriminants used
  - D_{VBF} and D_{Top+VV} are used to distinguish signal from backgrounds
  - Additional BDT (D_{ggF}) or kinematic cuts are used in control regions

- Profile likelihood fit with an unfolding method to extract the cross section

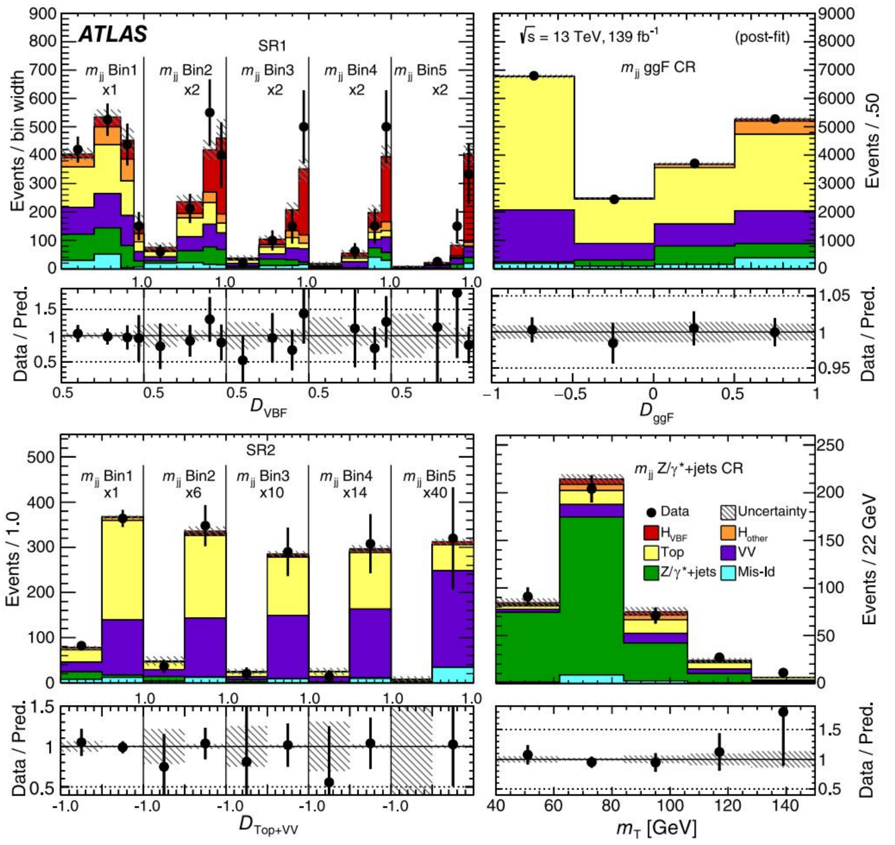

Differential XS in H→WW*: VBF Results

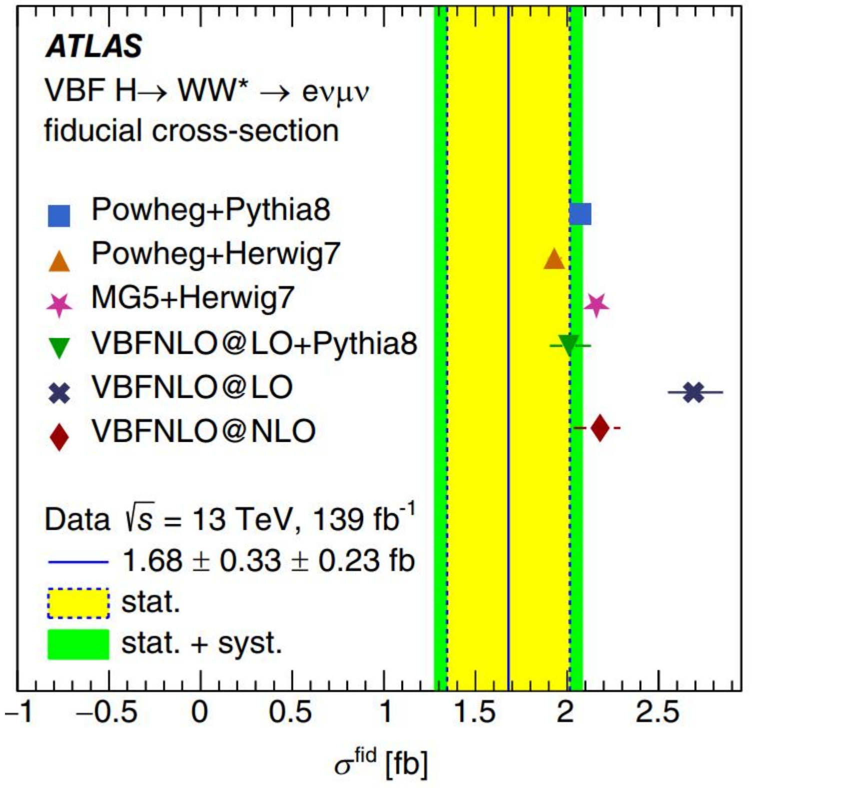

$$\sigma^{\text{fid}} = 1.68 \pm 0.40 \text{ fb} = 1.68 \pm 0.33\,(\text{stat}) \pm 0.23\,(\text{syst}) \text{ fb}.$$

- Statistical uncertainty dominant
- Measurements are consistent with the SM

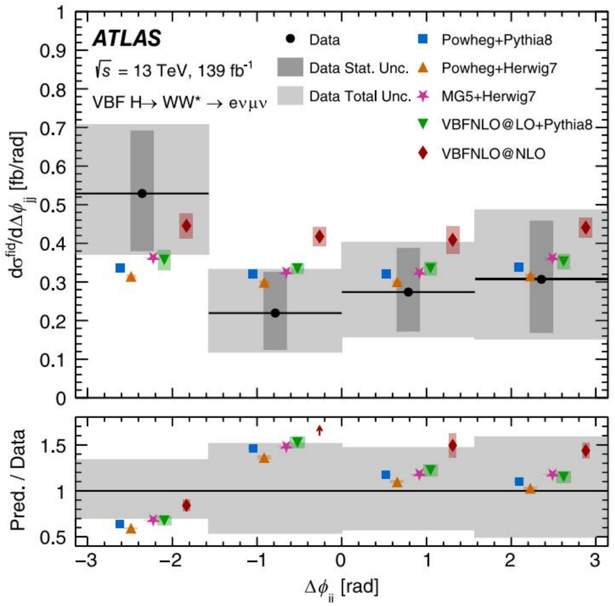

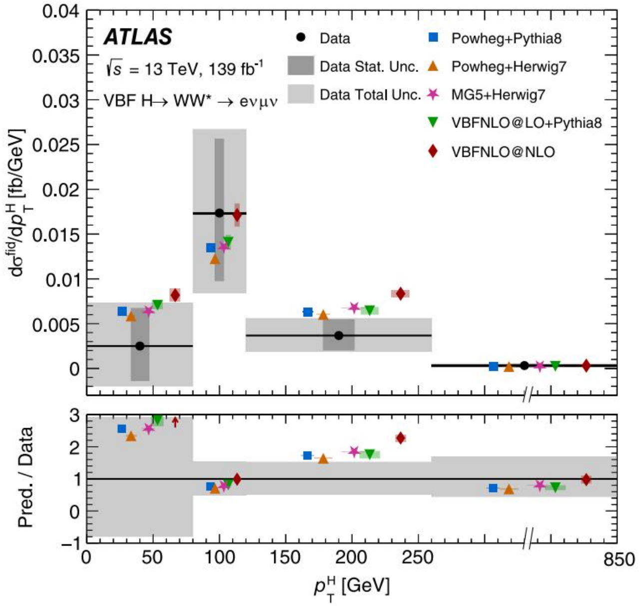

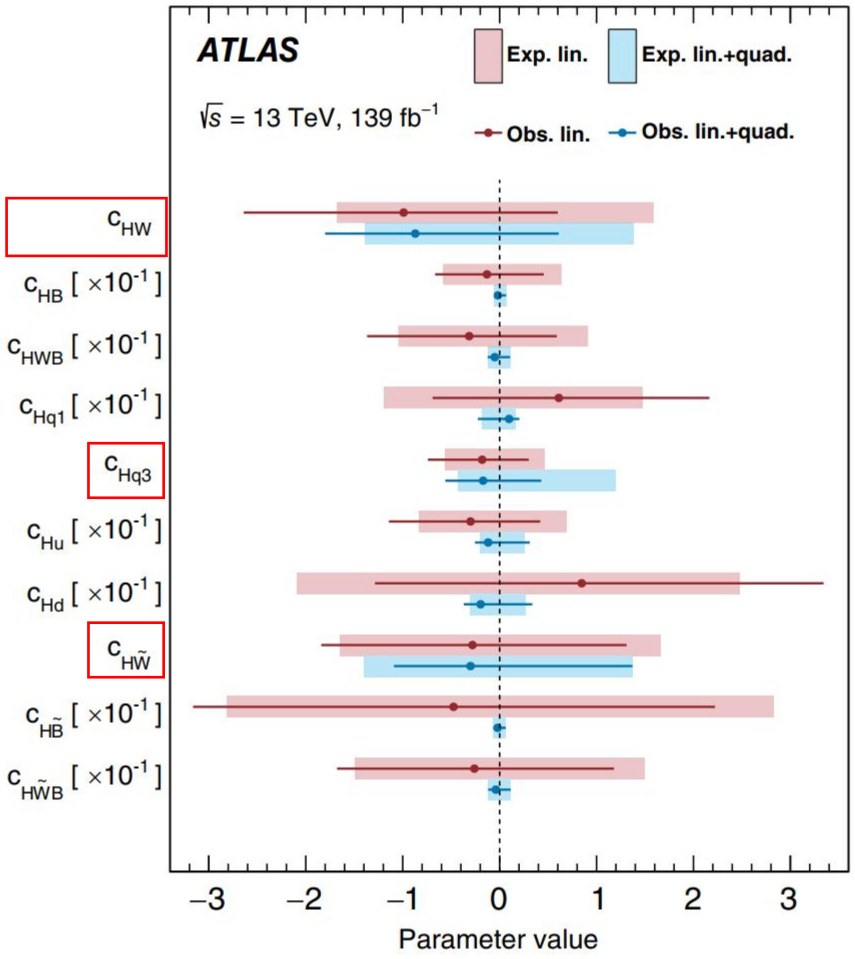

Differential cross sections used to constrain anomalous interactions

Most stringent constraint

Summary

- $H \rightarrow WW^*$ channels investigated with 139 fb^{-1} of data collected with the ATLAS detector @13TeV
  - Inclusive, STXS and differential cross section measurements are presented
  - All the measurements are in agreement with the SM predictions
  - The differential cross sections measurements are used to constrain the anomalous interactions
- Thanks to the increased statistics with full Run2 dataset, more finely-grained measurements are presented.

Stay tuned for more results to come from Run2 & Run3

Thanks

Backup

The importance of the Higgs boson

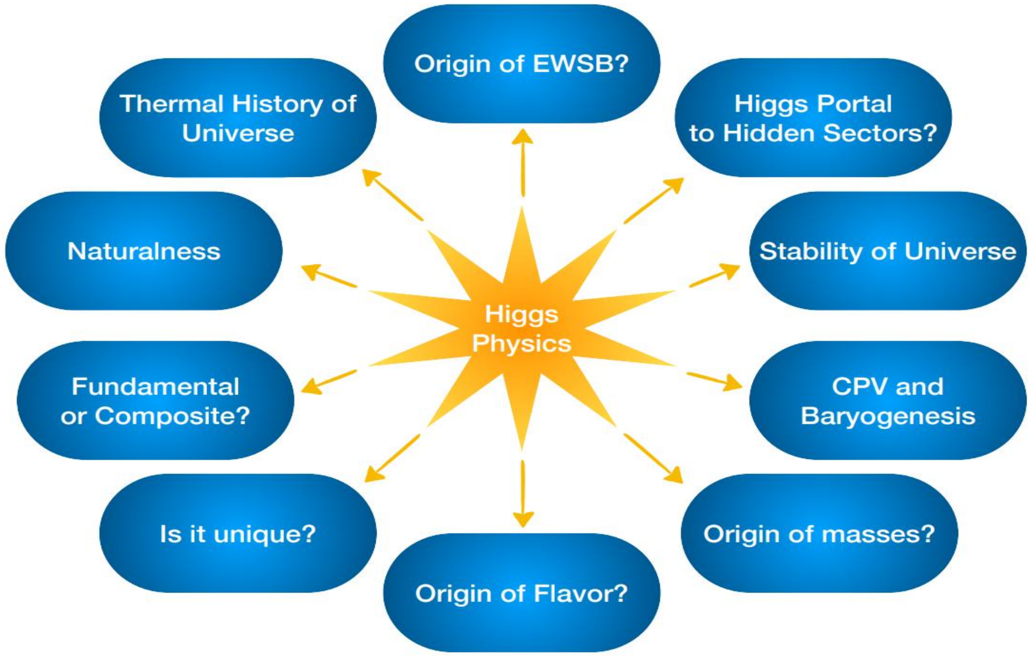

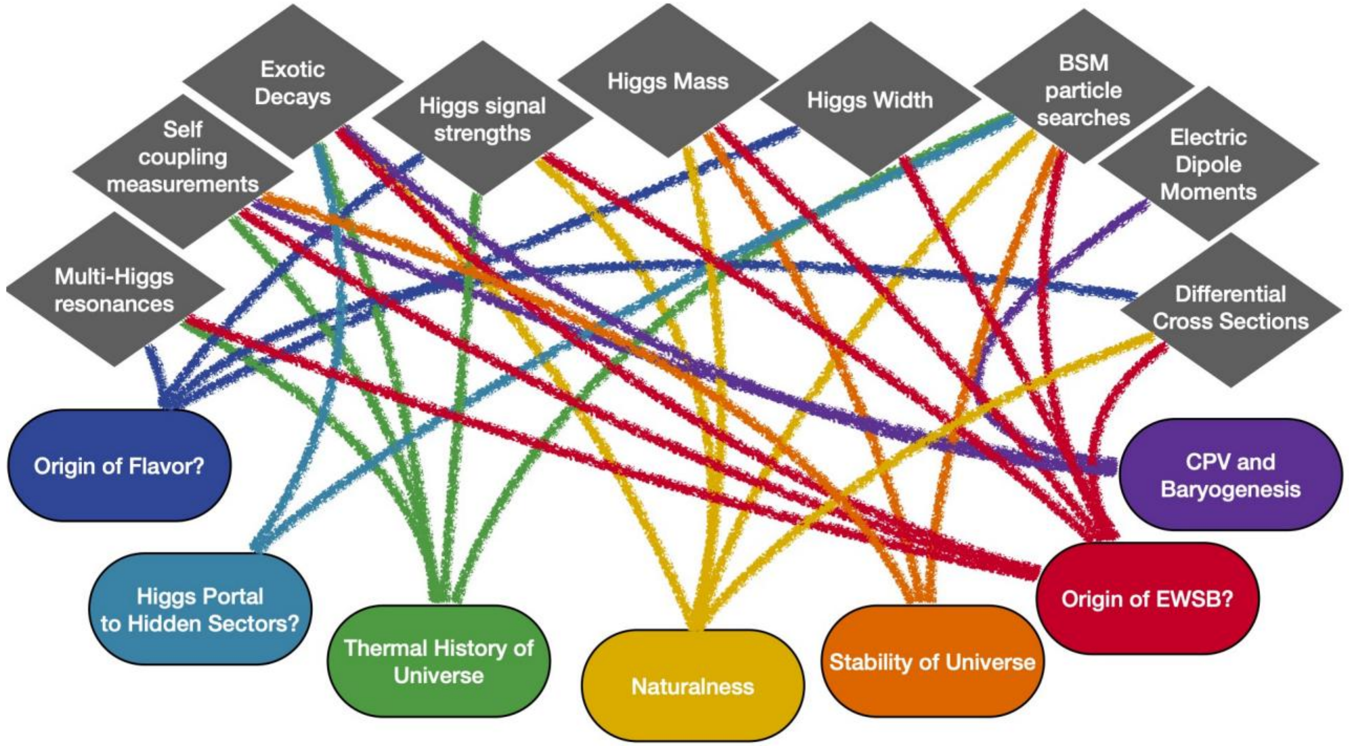

[arXiv: 2209.07510](https://arxiv.org/abs/2209.07510)

ggF & VBF H→WW*:　Samples

Process	Matrix element (alternative)	PDF set	UEPS model (alternative model)	Prediction order for total cross section
ggF H	POWHEG BOX2 [23–27] NNLOPS [26,30,43] (MG5_aMC@NLO) [49,86]	PDF4LHC15NNLO [57]	PYTHIA8 [28] (Herwig7) [48]	N^3LO QCD + NLO EW [11,33–42]
VBF H	POWHEG BOX2 [23–25,43] (MG5_aMC@NLO)	PDF4LHC15NLO	PYTHIA8 (Herwig7)	NNLO QCD + NLO EW [44–46]
VH excluding $gg \to ZH$	POWHEG BOX2	PDF4LHC15NLO	PYTHIA8	NNLO QCD + NLO EW [52–56]
$t\bar{t}H$	POWHEG BOX2	NNPDF3.0NLO	PYTHIA8	NLO [11]
$gg \to ZH$	POWHEG BOX2	PDF4LHC15NLO	PYTHIA8	NNLO QCD + NLO EW [87,88]
$qq \to WW$	Sherpa2.2.2 [69] (Q_{cut})	NNPDF3.0NNLO [50]	Sherpa2.2.2 [70,71,73–76] (Sherpa2.2.2 [71,72]; μ_q)	NLO [77,78,89]
$qq \to WWqq$	MG5_aMC@NLO [49]	NNPDF3.0NLO	PYTHIA8 (Herwig7)	LO
$gg \to WW/ZZ$	Sherpa2.2.2	NNPDF3.0NNLO	Sherpa2.2.2	NLO [90]
$WZ/V\gamma^*/ZZ$	Sherpa2.2.2	NNPDF3.0NNLO	Sherpa2.2.2	NLO [91]
$V\gamma$	Sherpa2.2.8 [69]	NNPDF3.0NNLO	Sherpa2.2.8	NLO [91]
VVV	Sherpa2.2.2	NNPDF3.0NNLO	Sherpa2.2.2	NLO
$t\bar{t}$	POWHEG BOX2 (MG5_aMC@NLO)	NNPDF3.0NLO	PYTHIA8 (Herwig7)	NNLO + NNLL [92–98]
Wt	POWHEG BOX2 (MG5_aMC@NLO)	NNPDF3.0NLO	PYTHIA8 (Herwig7)	NNLO [99,100]
Z/γ^*	Sherpa2.2.1 (MG5_aMC@NLO)	NNPDF3.0NNLO	Sherpa2.2.1	NNLO [79]

ggF & VBF H→WW*: SR definition

Category	$N_{\text{jet},(p_T>30\text{ GeV})}=0$ ggF	$N_{\text{jet},(p_T>30\text{ GeV})}=1$ ggF	$N_{\text{jet},(p_T>30\text{ GeV})}\geq 2$ ggF	$N_{\text{jet},(p_T>30\text{ GeV})}\geq 2$ VBF
Preselection	Two isolated, different-flavor leptons ($\ell = e, \mu$) with opposite charge $p_T^{\text{lead}} > 22$ GeV, $p_T^{\text{sublead}} > 15$ GeV $m_{\ell\ell} > 10$ GeV $p_T^{\text{miss}} > 20$ GeV			
Background rejection	$N_{b\text{-jet},(p_T>20\text{ GeV})} = 0$			
	$\Delta\phi_{\ell\ell,E_T^{\text{miss}}} > \pi/2$ $p_T^{\ell\ell} > 30$ GeV	$\max(m_T^{\ell}) > 50$ GeV	$m_{\tau\tau} < m_Z - 25$ GeV	
$H \to WW^* \to e\nu\mu\nu$ topology		$m_{\ell\ell} < 55$ GeV $\Delta\phi_{\ell\ell} < 1.8$	Fail central jet veto or fail outside lepton veto $\lvert m_{jj} - 85\rvert > 15$ GeV or $\Delta y_{jj} > 1.2$	Central jet veto outside lepton veto $m_{jj} > 120$ GeV
Discriminating fit variable		m_T		DNN

Calculated by using collinear approximation method

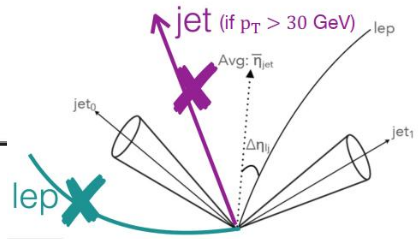

ggF & VBF H→WW*: CR definition

<table>
<tr><th>CR</th><th>$N_{\text{jet},(p_T>30\text{ GeV})} = 0$ ggF</th><th>$N_{\text{jet},(p_T>30\text{ GeV})} = 1$ ggF</th><th>$N_{\text{jet},(p_T>30\text{ GeV})} \geq 2$ ggF</th><th>$N_{\text{jet},(p_T>30\text{ GeV})} \geq 2$ VBF</th></tr>
<tr><td>$qq \to WW$</td><td colspan="3">$N_{b\text{-jet},(p_T>20\text{ GeV})} = 0$</td><td></td></tr>
<tr><td></td><td>$\Delta\phi_{\ell\ell,E_T^{\text{miss}}} > \pi/2$</td><td colspan="2">$m_{\ell\ell} > 80$ GeV</td><td></td></tr>
<tr><td></td><td>$p_T^{\ell\ell} > 30$ GeV
$55 < m_{\ell\ell} < 110$ GeV
$\Delta\phi_{\ell\ell} < 2.6$</td><td>$|m_{\tau\tau} - m_Z| > 25$ GeV
$\max(m_T^\ell) > 50$ GeV</td><td>$m_{\tau\tau} < m_Z - 25$ GeV
$m_{T2} > 165$ GeV
Fail central jet veto or fail outside lepton veto
$|m_{jj} - 85| > 15$ GeV
or $\Delta y_{jj} > 1.2$</td><td>$m_{T2}^2 = \min_{\not{p}_1+\not{p}_2=\not{p}_T} [\max\{m_T^2(p_T^a, \not{p}_1), m_T^2(p_T^b, \not{p}_2)\}],$</td></tr>
<tr><td>$t\bar{t}/Wt$</td><td>$N_{b\text{-jet},(20<p_T<30\text{ GeV})} > 0$
$\Delta\phi_{\ell\ell,E_T^{\text{miss}}} > \pi/2$
$p_T^{\ell\ell} > 30$ GeV
$\Delta\phi_{\ell\ell} < 2.8$</td><td>$N_{b\text{-jet},(p_T>30\text{ GeV})} = 1$
$N_{b\text{-jet},(20<p_T<30\text{ GeV})} = 0$
$\max(m_T^\ell) > 50$ GeV</td><td>$N_{b\text{-jet},(p_T>20\text{ GeV})} = 0$
$m_{\tau\tau} < m_Z - 25$ GeV
$m_{\ell\ell} > 80$ GeV
$\Delta\phi_{\ell\ell} < 1.8$
$m_{T2} < 165$ GeV
Fail central jet veto or fail outside lepton veto
$|m_{jj} - 85| > 15$ GeV
or $\Delta y_{jj} > 1.2$</td><td>$N_{b\text{-jet},(p_T>20\text{ GeV})} = 1$
Central jet veto
outside lepton veto</td></tr>
<tr><td>Z/γ^*</td><td colspan="4">$N_{b\text{-jet},(p_T>20\text{ GeV})} = 0$</td></tr>
<tr><td></td><td colspan="2">$m_{\ell\ell} < 80$ GeV
no p_T^{miss} requirement</td><td>$m_{\ell\ell} < 55$ GeV</td><td>$m_{\ell\ell} < 70$ GeV</td></tr>
<tr><td></td><td>$\Delta\phi_{\ell\ell} > 2.8$</td><td colspan="2">$m_{\tau\tau} > m_Z - 25$ GeV</td><td>$|m_{\tau\tau} - m_Z| \leq 25$ GeV</td></tr>
<tr><td></td><td></td><td>$\max(m_T^\ell) > 50$ GeV</td><td>Fail central jet veto or fail outside lepton veto
$|m_{jj} - 85| > 15$ GeV or
$\Delta y_{jj} > 1.2$</td><td>central jet veto
outside lepton veto</td></tr>
</table>

ggF & VBF H→WW*： Results

Source	$\frac{\Delta\sigma_{\mathrm{ggF+VBF}}\cdot\mathcal{B}_{H\to WW^*}}{\sigma_{\mathrm{ggF+VBF}}\cdot\mathcal{B}_{H\to WW^*}}$ [%]	$\frac{\Delta\sigma_{\mathrm{ggF}}\cdot\mathcal{B}_{H\to WW^*}}{\sigma_{\mathrm{ggF}}\cdot\mathcal{B}_{H\to WW^*}}$ [%]	$\frac{\Delta\sigma_{\mathrm{VBF}}\cdot\mathcal{B}_{H\to WW^*}}{\sigma_{\mathrm{VBF}}\cdot\mathcal{B}_{H\to WW^*}}$ [%]
Data statistical uncertainties	4.6	5.1	15
Total systematic uncertainties	9.5	11	18
MC statistical uncertainties	3.0	3.8	4.9
Experimental uncertainties	5.2	6.3	6.7
Flavor tagging	2.3	2.7	1.0
Jet energy scale	0.9	1.1	3.7
Jet energy resolution	2.0	2.4	2.1
$E_{\mathrm{T}}^{\mathrm{miss}}$	0.7	2.2	4.9
Muons	1.8	2.1	0.8
Electrons	1.3	1.6	0.4
Mis-Id extrapolation factors	2.1	2.4	0.8
Pileup	2.4	2.5	1.3
Luminosity	2.1	2.0	2.2
Theoretical uncertainties	6.8	7.8	16
ggF	3.8	4.3	4.6
VBF	3.2	0.7	12
WW	3.5	4.2	5.5
Top	2.9	3.8	6.4
$Z\tau\tau$	1.8	2.3	1.0
Other VV	2.3	2.9	1.5
Other Higgs	0.9	0.4	0.4
Background normalizations	3.6	4.5	4.9
WW	2.2	2.8	0.6
Top	1.9	2.3	3.4
$Z\tau\tau$	2.7	3.1	3.4
Total	10	12	23

ggF: exp (b-jet ID, JER, Mis-id) and theory (jet multi, PS) comparable

VBF: (ME Matching, PS) + E_TMiss

WW and top related uncertainties dominant

VBF $H \to WW^*$: Deep Neural Network (DNN)

- More complex final state
- DNN inputs:
  (after preselection, $m_{\tau\tau} < m_Z - 25$ GeV & b-veto)
  m_{jj}, Δy_{jj}, $\sum_\ell C_\ell$ ($C_\ell = |2\eta_\ell - \sum \eta_j| / \Delta\eta_{jj}$)
  $p_T^{j0,j1,j2}$, $m_{\ell_i j_j}$, $m_{\ell\ell}$,
  $\Delta\phi_{\ell\ell}$, m_T, p_T^{tot}, E_T^{miss} significance

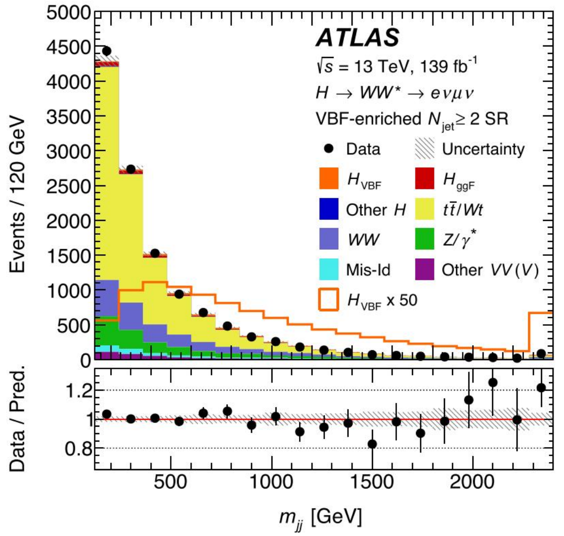

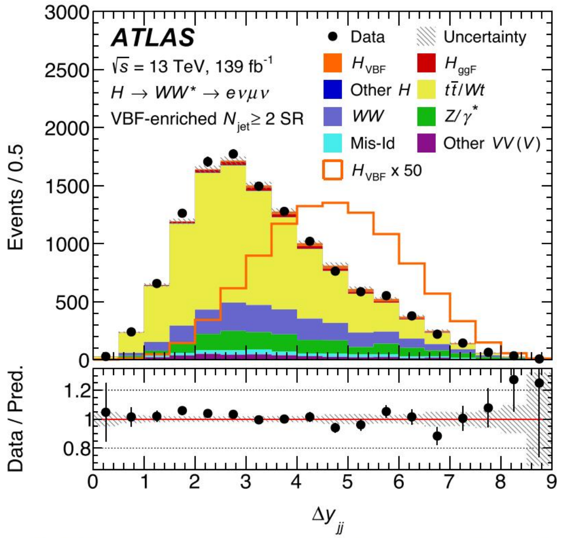

- Training target: VBF vs. non-H + ggF
  → reduce ggF/VBF interplay

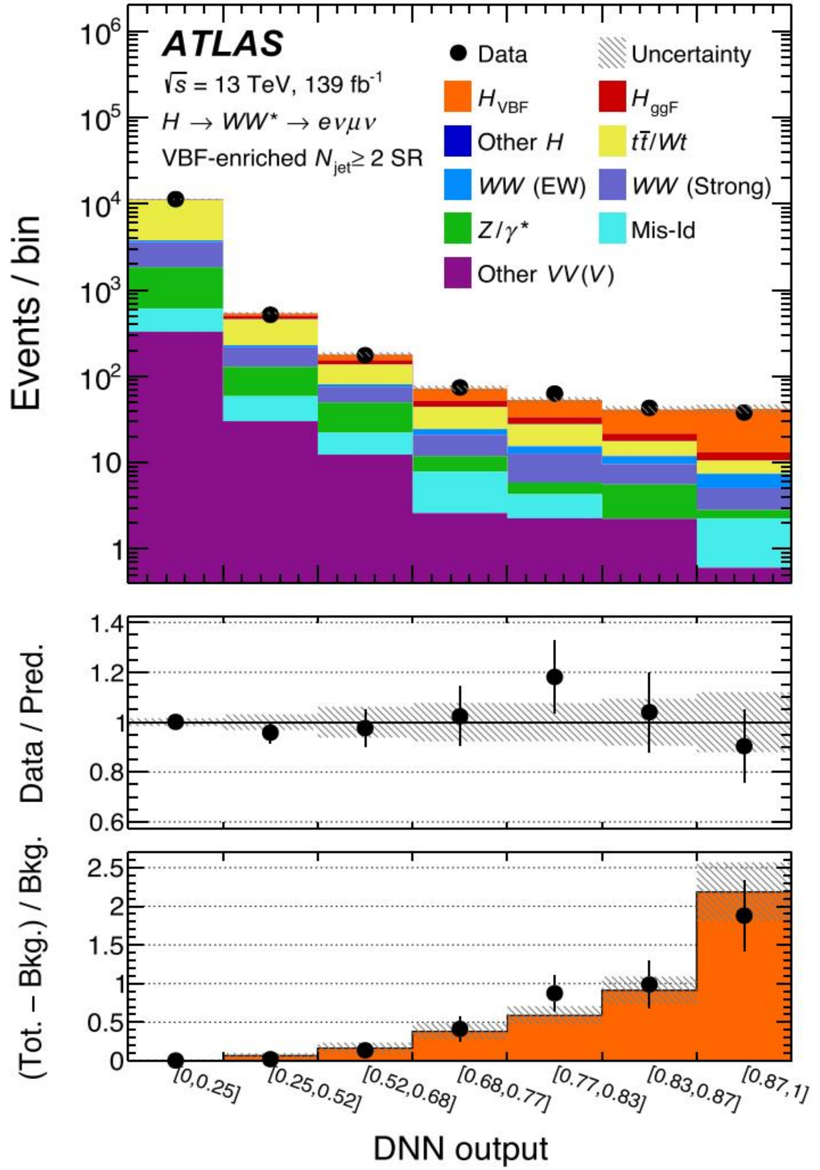

ggF & VBF H→WW*

STXS bin $(\sigma_i \cdot \mathcal{B}_{H\to WW^*})$	Value (fb)	Uncertainty (fb): Total	Statistical	Experimental systematics	Signal Theory	Background Theory	SM prediction (fb)
ggH-0j, low p_T^H $p_T^H < 200$ GeV	7100	$^{+950}_{-910}$	$^{+480}_{-470}$	$^{+570}_{-530}$	$^{+320}_{-260}$	$^{+490}_{-480}$	5870 ± 390
ggH-1j, very low p_T^H $p_T^H < 60$ GeV	1140	$^{+800}_{-820}$	$^{+420}_{-410}$	$^{+380}_{-380}$	$^{+80}_{-70}$	$^{+570}_{-600}$	1400 ± 190
ggH-1j, low p_T^H $60 \le p_T^H < 120$ GeV	540	$^{+470}_{-470}$	$^{+310}_{-310}$	$^{+230}_{-230}$	$^{+42}_{-47}$	$^{+270}_{-280}$	970 ± 150
ggH-1j, medium p_T^H $120 \le p_T^H < 200$ GeV	230	$^{+130}_{-120}$	$^{+100}_{-100}$	$^{+60}_{-60}$	$^{+10}_{-10}$	$^{+50}_{-50}$	160 ± 30
ggH-2j, low p_T^H $p_T^H < 200$ GeV	1610	$^{+900}_{-890}$	$^{+440}_{-440}$	$^{+430}_{-420}$	$^{+300}_{-150}$	$^{+640}_{-650}$	1010 ± 220
ggH, high p_T^H $p_T^H \ge 200$ GeV	260	$^{+100}_{-100}$	$^{+80}_{-80}$	$^{+40}_{-40}$	$^{+40}_{-20}$	$^{+40}_{-40}$	122 ± 31
EW qqH-2j, low m_{jj}-low p_T^H $350 \le m_{jj} < 700$ GeV, $p_T^H < 200$ GeV	6	$^{+63}_{-62}$	$^{+46}_{-42}$	$^{+31}_{-34}$	$^{+11}_{-14}$	$^{+24}_{-26}$	109 ± 7
EW qqH-2j, medium m_{jj}-low p_T^H $700 \le m_{jj} < 1000$ GeV, $p_T^H < 200$ GeV	31	$^{+35}_{-33}$	$^{+30}_{-27}$	$^{+15}_{-14}$	$^{+8}_{-7}$	$^{+11}_{-10}$	56 ± 4
EW qqH-2j, high m_{jj}-low p_T^H $1000 \le m_{jj} < 1500$ GeV, $p_T^H < 200$ GeV	60	$^{+26}_{-23}$	$^{+23}_{-21}$	$^{+7}_{-7}$	$^{+9}_{-5}$	$^{+5}_{-5}$	51 ± 4
EW qqH-2j, very high m_{jj}-low p_T^H $m_{jj} \ge 1500$ GeV, $p_T^H < 200$ GeV	57	$^{+20}_{-18}$	$^{+18}_{-17}$	$^{+5}_{-5}$	$^{+3}_{-3}$	$^{+4}_{-4}$	50 ± 4
EW qqH-2j, high p_T^H $m_{jj} \ge 350$ GeV, $p_T^H \ge 200$ GeV	37	$^{+16}_{-14}$	$^{+14}_{-13}$	$^{+4}_{-3}$	$^{+4}_{-3}$	$^{+3}_{-3}$	32 ± 1

Cross sections in each STXS bins

VH H→WW*: Signal strength and significance

Channel	POI / Z_0	Expected	Observed
Opposite-sign 2ℓ	μ_{VH}	$1.00^{+1.02}_{-0.98}$	$1.94^{+1.07}_{-1.02}$
	Z_0	1.0	1.9
Same-sign 2ℓ	μ_{WH}	$1.00^{+0.61}_{-0.60}$	-0.08 ± 0.58
	Z_0	1.6	0.0
3ℓ	μ_{WH}	$1.00^{+0.44}_{-0.40}$	$0.64^{+0.42}_{-0.37}$
	Z_0	2.8	1.8
4ℓ	μ_{ZH}	$1.00^{+0.47}_{-0.39}$	$1.59^{+0.54}_{-0.47}$
	Z_0	3.1	4.5
Combined 1-POI	μ_{VH}	$1.00^{+0.27}_{-0.25}$	$0.92^{+0.25}_{-0.23}$
	Z_0	4.7	4.6
Combined 2-POI	μ_{WH}	$1.00^{+0.35}_{-0.33}$	$0.45^{+0.32}_{-0.30}$
	μ_{ZH}	$1.00^{+0.47}_{-0.39}$	$1.64^{+0.55}_{-0.47}$
	Z_0^{WH}	3.3	1.5
	Z_0^{ZH}	3.1	4.6

VH H→WW*: Breakdown

Source	$\frac{\Delta(\sigma_{VH}\times\mathcal{B}_{H\to WW^*})}{\sigma_{VH}\times\mathcal{B}_{H\to WW^*}}$ [%]	$\frac{\Delta(\sigma_{WH}\times\mathcal{B}_{H\to WW^*})}{\sigma_{WH}\times\mathcal{B}_{H\to WW^*}}$ [%]	$\frac{\Delta(\sigma_{ZH}\times\mathcal{B}_{H\to WW^*})}{\sigma_{ZH}\times\mathcal{B}_{H\to WW^*}}$ [%]
Statistical uncertainties in data	22.3	57.9	28.4
Systematic uncertainties	13.3	36.6	9.9
Statistical uncertainties in simulation	6.4	14.4	5.9
Experimental systematic uncertainties	5.2	9.8	6.0
Electrons	1.2	1.8	1.6
Muons	2.5	2.8	4.1
Jet energy scale	0.7	2.3	0.5
Jet energy resolution	0.6	2.8	0.6
Flavour tagging	0.9	1.4	0.8
Missing transverse momentum	0.6	0.4	0.9
Pile-up	1.1	1.5	0.8
Luminosity	2.3	2.4	2.1
Mis-identified leptons	2.9	7.1	2.7
Charge-flip electrons	1.5	4.5	0.1
Theoretical uncertainties	6.0	18.6	4.7
WH	2.3	2.8	0.1
ZH	0.7	0.7	3.4
WW	1.0	3.3	0.3
$W(Z/\gamma^*)$ 0-jet	3.2	11.3	0.3
$W(Z/\gamma^*)$ $\geq$1-jets	0.2	0.8	0.4
$Z(Z/\gamma^*)$	0.8	1.5	0.6
VVV	2.4	12.7	0.3
Top	2.9	5.5	2.5
Z+jets	1.8	3.4	1.5
RNN shape uncertainty for $W(Z/\gamma^*)$	8.8	27.3	0.3
Floating normalisations	0.1	0.2	0.1
Total	26.0	71.0	30.1

VH H→WW*: Same sign 2l channel

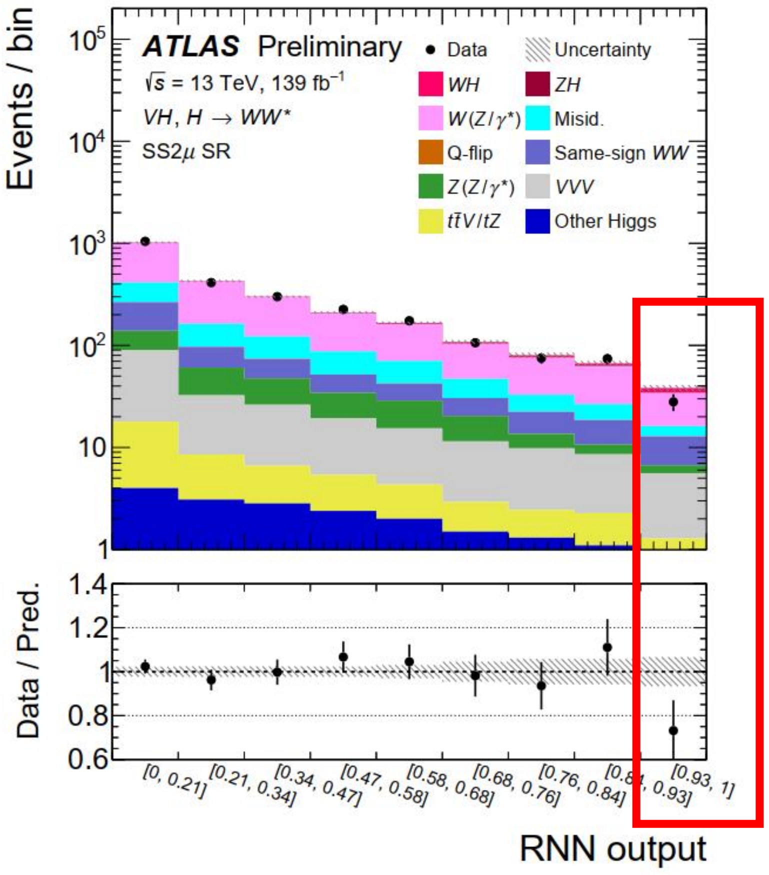

(a) SS2μ

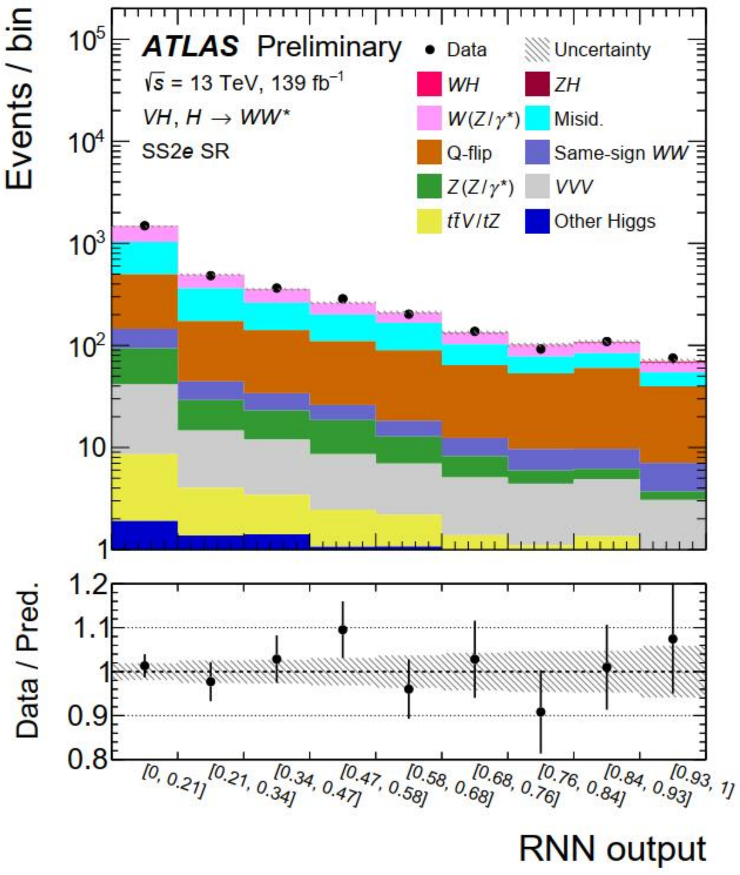

(b) SS2e

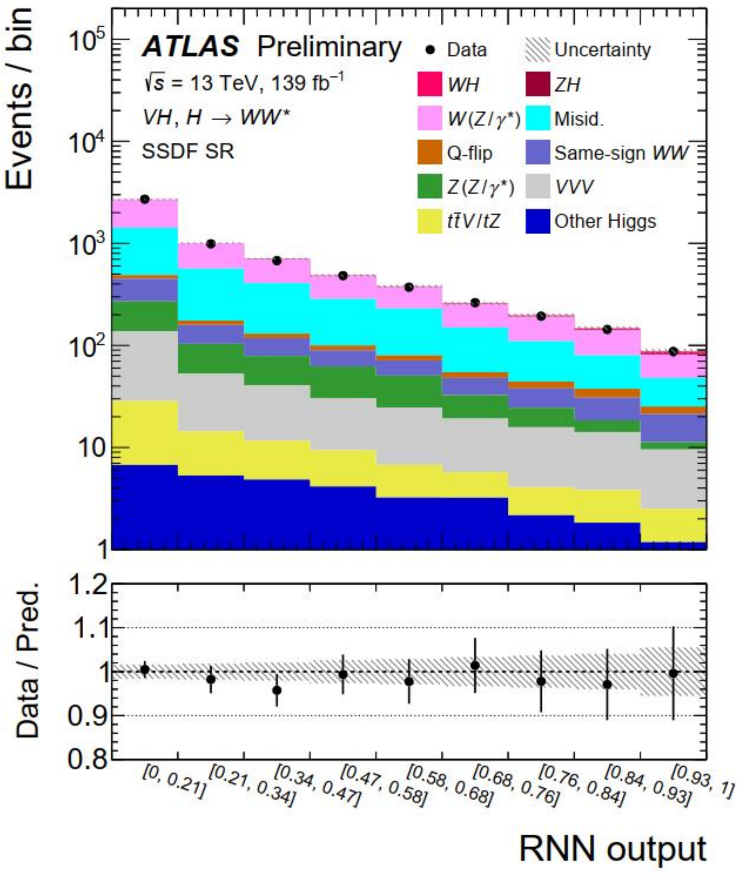

(c) SSDF

VBF H→WW* Differential XS: Break down

	Uncertainty [%]	Uncertainty range [%]				
Source	σ^{fid}	p_{T}^{H}	$p_{\text{T}}^{\ell\ell}$, $p_{\text{T}}^{\ell_1}$, $p_{\text{T}}^{\ell_2}$, $\|\Delta y_{\ell\ell}\|$, $\|\Delta\phi_{\ell\ell}\|$, $\cos(\theta_{\eta}^{*})$	$m_{\ell\ell}$	$p_{\text{T}}^{j_1}$, $p_{\text{T}}^{j_2}$, $\|\Delta y_{jj}\|$, $\Delta\phi_{jj}$	m_{jj}
Signal modeling	5	< 1–7	< 1–7	< 1–19	< 1–8	2–7
Signal parton shower	< 1	< 1–2	< 1–1.8	< 1–10	< 1–1.8	< 1–7
$t\bar{t}$ modeling	6	1.7–30	3–13	3–80	3–10	1.2–70
WW modeling	4	< 1–12	3–11	2–90	3–10	3–40
$Z/\gamma^* +$ jets modeling	4	< 1–19	2–18	4–30	3–13	2–50
ggF modeling	5	4.0–28	3.4–10	2.6–12	2.3–9.0	1.4–86
Mis-Id background	< 1	< 1–12	1.1–5	< 1–19	1–3	< 1–40
Jets & Pile-up & $E_{\text{T}}^{\text{miss}}$	5	8–60	6–30	6–120	9–30	9–130
b-tagging	< 1	< 1–9	< 1–3	< 1–19	1.1–3	< 1–40
Leptons	1.5	3–17	2–9	1.2–13	1.7–7	< 1–16
Luminosity	1.5	1.7–2	1.3–1.9	< 1–4	1.5–2	< 1–1.9
MC statistics	5	10–40	6–30	6–180	8–30	7–90
Total systematics	13	19–90	13–60	12–180	15–50	15–200
Data statistics	20	50–160	30–110	30–400	40–100	50–300
Total uncertainty	23	50–190	40–120	30–500	40–100	50–400

VBF H→WW* Differential XS

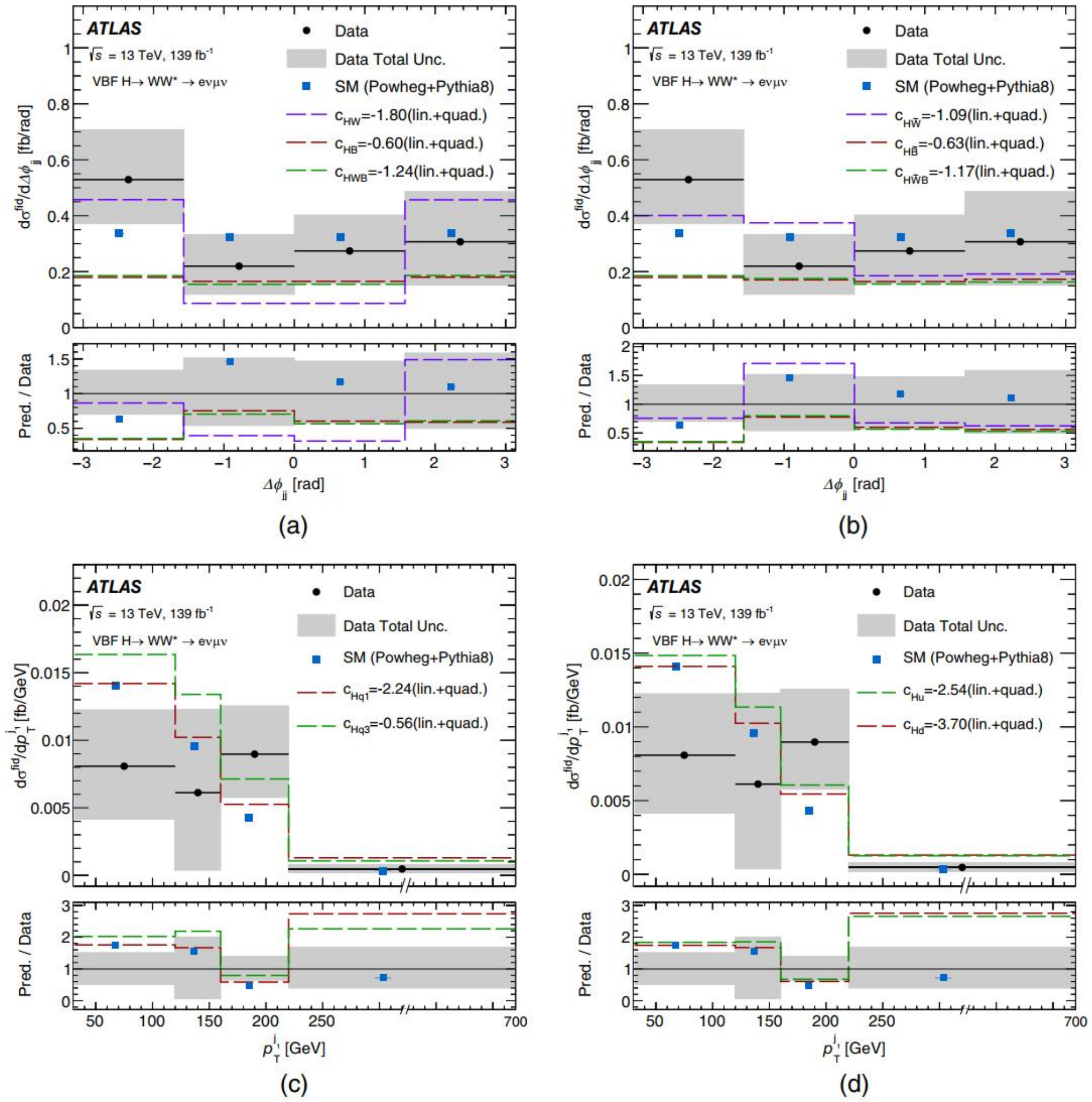

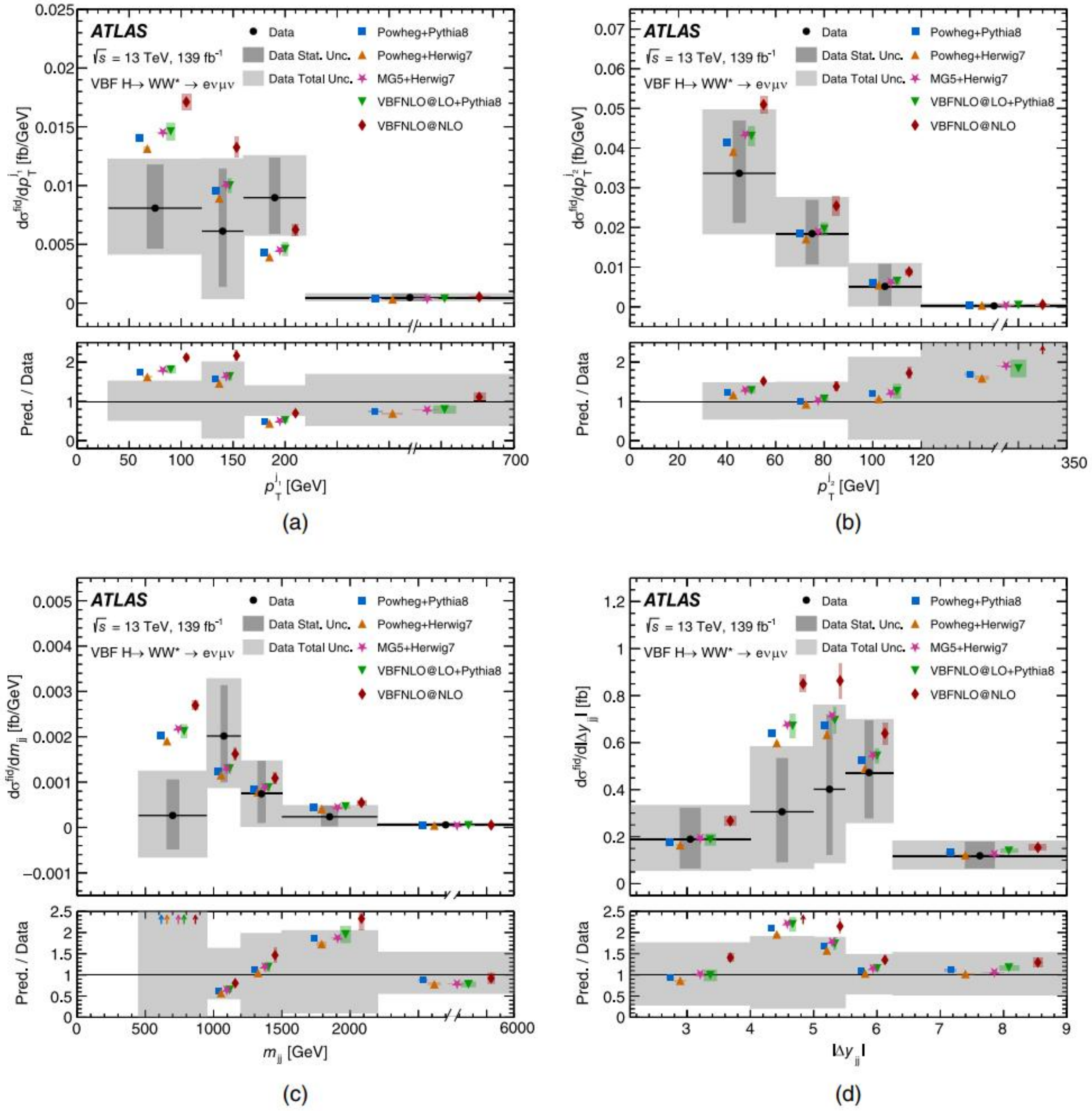

VBF H→WW* Differential XS

Wilson coefficients	Operator structure	Fit distr	Paramater order	95% Confidence interval [TeV^{-2}] Expected	Observed
c_{HW}	$H^\dagger H W^n_{\mu\nu} W^{n\mu\nu}$	$\Delta\phi_{jj}$	lin	[−1.7, 1.6]	[−2.6, 0.60]
			lin + quad	[−1.4, 1.4]	[−1.8, 0.61]
c_{HB}	$H^\dagger H B_{\mu\nu} B^{\mu\nu}$	$\Delta\phi_{jj}$	lin	[−5.9, 6.4]	[−6.7, 4.6]
			lin + quad	[−0.59, 0.66]	[−0.60, 0.66]
c_{HWB}	$H^\dagger \tau^n H W^n_{\mu\nu} B^{\mu\nu}$	$\Delta\phi_{jj}$	lin	[−10, 9]	[−14, 5.9]
			lin + quad	[−1.2, 1.1]	[−1.2, 1.1]
c_{Hq1}	$(H^\dagger i\overleftrightarrow{D}_\mu H)(\bar{q}\gamma^\mu q)$	p_T^{j1}	lin	[−12, 15]	[−6.9, 22]
			lin + quad	[−1.9, 1.7]	[−2.2, 2.0]
c_{Hq3}	$(H^\dagger i\overleftrightarrow{D}^n_\mu H)(\bar{q}\tau^n\gamma^\mu q)$	p_T^{j1}	lin	[−0.56, 0.47]	[−0.74, 0.30]
			lin + quad	[−0.43, 1.2]	[−0.56, 0.43]
c_{Hu}	$(H^\dagger i\overleftrightarrow{D}_\mu H)(\bar{u}\gamma^\mu u)$	p_T^{j1}	lin	[−8.3, 6.9]	[-11, 4.2]
			lin + quad	[−2.0, 2.6]	[−2.5, 3.1]
c_{Hd}	$(H^\dagger i\overleftrightarrow{D}_\mu H)(\bar{d}\gamma^\mu d)$	p_T^{j1}	lin	[−21, 25]	[−13, 33]
			lin + quad	[−3.0, 2.7]	[−3.7, 3.4]
$c_{H\tilde{W}}$	$H^\dagger H \tilde{W}^n_{\mu\nu} W^{n\mu\nu}$	$\Delta\phi_{jj}$	lin	[−1.7, 1.7]	[−1.8, 1.3]
			lin + quad	[−1.4, 1.4]	[−1.1, 1.4]
$c_{H\tilde{B}}$	$H^\dagger H \tilde{B}_{\mu\nu} B^{\mu\nu}$	$\Delta\phi_{jj}$	lin	[−28, 28]	[−32, 22]
			lin + quad	[−0.62, 0.62]	[−0.63, 0.63]
$c_{H\tilde{W}B}$	$H^\dagger \tau^n H \tilde{W}^n_{\mu\nu} B^{\mu\nu}$	$\Delta\phi_{jj}$	lin	[−15, 15]	[−17, 12]
			lin + quad	[−1.2, 1.1]	[−1.2, 1.1]

The parametrizations for cHW~B and cHu are found to be poorly described by a linear and a linear plus quadratic function of the Wilson coefficients for values beyond the sensitivity of the measurement, i.e., outside the limit ranges. This effect is due to a dependence of the fiducial selection efficiency on the EFT parameters for extreme values of these couplings and not to a data unfolding bias. The associated bias was studied and its effect was assigned as an uncertainty to the EFT parametrization for those couplings. It was found to have negligible impact on the limits, i.e., about an order of magnitude smaller than the impact of systematic uncertainties assigned to the signal modeling

ggF H→WW* Differential XS： Tikhonov regularization

A Tikhonov regularization term is included in the likelihood as a penalty term： Sov. Math. Dokl. 5, 1035/1038 (1963)

$$P(\vec{x}) = \exp\left(-\tau \cdot \left(\sum_{i=2}^{N_{\text{bin}}-1} ((x_{i-1} - x_i) - (x_i - x_{i+1}))^2\right)\right)$$

regularization parameter τ

with x being the quantity for which the curvature should be regularized. For this analysis, the measured particle-level signal strength, $x_i = {s_i^t}/{s_i^{t,exp}}$, is chosen as the regularized quantity Eur. Phys. J. C 80, 942 (2020)

The choice of a value for the regularization parameter τ is a trade-off between minimizing statistical fluctuations on the one hand, and the potential bias induced by adding an artificial constraint to the measurement on the other.

ggF H→WW* Differential XS

Table 6 Relative cross section uncertainties broken down for each bin in p_T^H

Contribution	0 – 30 GeV	30 – 60 GeV	60 – 120 GeV	120 – 1000 GeV
Total relative uncertainty	19	51	108	62
Total systematic uncertainty	17	41	81	45
Statistical uncertainties from data	8.5	29	72	43
Statistical uncertainties from simulation	6.2	15	17	18
Experimental systematic uncertainty	10	24	58	31
Flavour tagging	4.9	6.1	13	18
Jet Energy Scale	4.9	17	30	21
Jet Energy Resolution	4.8	8.4	12	10
Missing transverse energy	4.6	8.2	11	8.2
Muons	4.6	4.2	4.8	2.3
Electrons	3.2	2.2	2.5	1.1
Misidentified objects	3.9	10	3.3	1.3
Pile-up	3.8	1.2	6.9	4.4
Luminosity	2.7	4.5	3.5	2.8
Systematic uncertainty from theory	11	27	23	25
On gluon-fusion production	6.1	7.1	4.7	5.2
On Vector Boson Fusion production	2.4	1.8	2.7	3.2
On top quark production	4.3	20	18	21
On decays of $Z \to \tau\tau$	4.2	5.9	2.2	3.9
On the WW background	7.3	10	12	6.0
On other diboson processes	5.9	14	7.8	8.8
Background normalization factors	2.3	0.7	0.9	0.6

The uncertainties with the largest impact on the results include uncertainties related to jet and muon reconstruction.

Theory uncertainties associated with the top-quark and W W backgrounds,

and with the difficulty of modelling V γ processes also play a leading role

data-driven background estimates for misidentified objects

ggF H→WW* Differential XS

Variable	Data statistical (%)	MC statistical (%)	Experimental (%)	Theory (%)
$y_{\ell\ell}$	14–22	5.3–10	6.9–15	5.9–15
$p_{\mathrm{T}}^{\ell\ell}$	15–29	6.4–14	8.2–31	6.8–27
$p_{\mathrm{T}}^{\ell 0}$	13–28	6.3–13	9.3–28	14–34
$\Delta\phi_{\ell\ell}$	11–39	6.1–18	7.8–22	13–27
y_{j0}	23–51	12–26	21–54	26–58
$\cos\theta^*$	11–15	5.8–7.6	8.5–11	8.9–14
p_{T}^{H}	8.5–72	6.2–18	10–58	12–27
$m_{\ell\ell}$	12–25	5.6–11	7.5–15	7.3–20
$y_{\ell\ell}$ vs N_{jet}	9.0–62	3.9–25	8.0–20	5.0–53
$p_{\mathrm{T}}^{\ell\ell}$ vs N_{jet}	9.8–36	4.7–20	12–41	9.9–50
$p_{\mathrm{T}}^{\ell 0}$ vs N_{jet}	9.6–50	5.8–20	10–35	9.4–74
$\Delta\phi_{\ell\ell}$ vs N_{jet}	9.6–65	5.6–18	6.8–31	14–74
$\cos\theta^*$ vs N_{jet}	13–50	6.8–25	7.7–39	8.9–58
$m_{\ell\ell}$ vs N_{jet}	12–152	5.7–44	8.9–58	7.2–82

$\cos\theta^* = |\tanh(\frac{1}{2}\Delta\eta_{\ell\ell})|$ $\Delta\eta_{\ell\ell}$ is the lepton pseudorapidity difference

Tikhonov-regularized in-likelihood unfolding algorithm VS iterative Bayesian unfolding

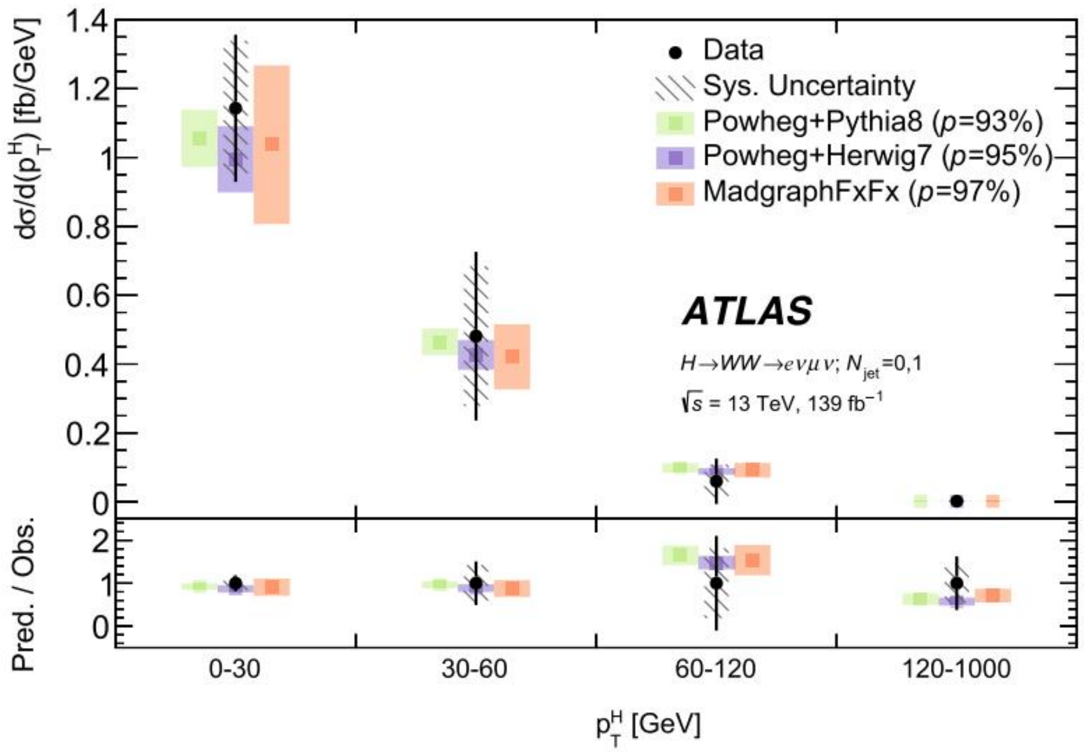

Tikhonov-regularized in-likelihood unfolding

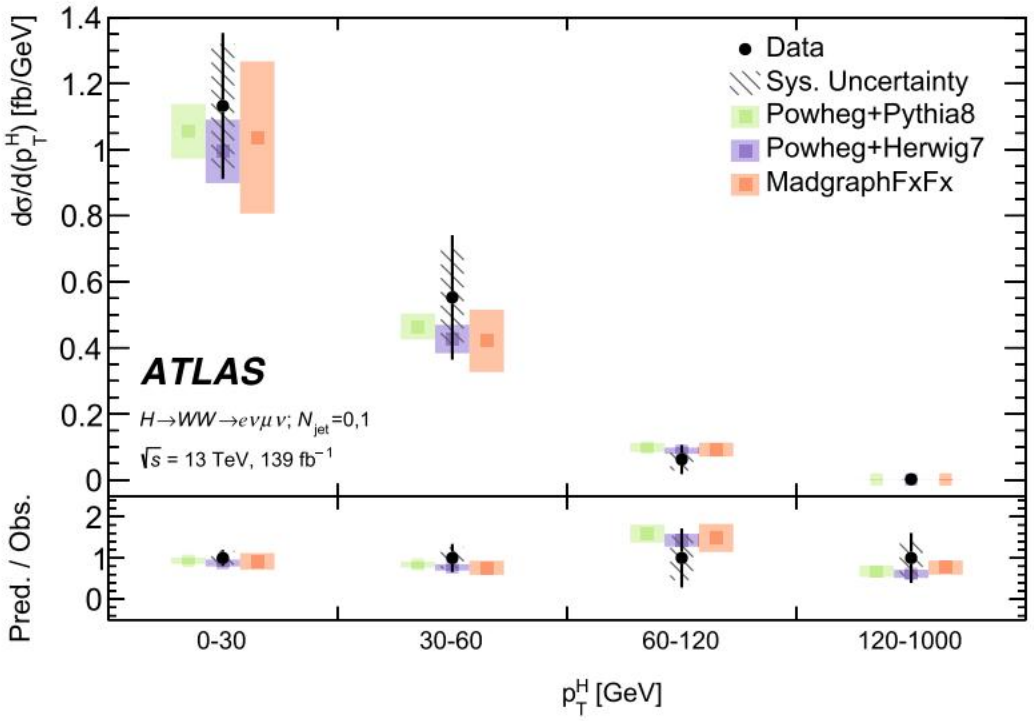

iterative Bayesian unfolding

ggF H→WW* Differential XS